

The Solar Neighborhood. XLIII: Discovery of New Nearby Stars with $\mu < 0.18'' \text{ yr}^{-1}$ (TINYMO sample)

ADRIC R. RIEDEL,¹ MICHELE L. SILVERSTEIN,² TODD J. HENRY,³ WEI-CHUN JAO,² JENNIFER G. WINTERS,⁴
JOHN P. SUBASAVAGE,⁵ LISON MALO,⁶ AND NIGEL C. HAMBLY⁷

¹*Space Telescope Science Institute, Baltimore, MD 21218*

²*Physics and Astronomy Department, Georgia State University, Atlanta, GA 30302*

³*RECONS Institute, Chambersburg, PA*

⁴*Harvard-Smithsonian Center for Astrophysics, Cambridge, MA 02138*

⁵*US Naval Observatory Flagstaff Station, Flagstaff, AZ 86005*

⁶*Canada-France-Hawaii Telescope, Kamuela, HI 96743*

⁷*Institute for Astronomy, University of Edinburgh, Blackford Hill, Edinburgh, EH9 3HJ, Scotland, UK*

ABSTRACT

We have conducted a novel search of most of the southern sky for nearby red dwarfs having low proper motions, with specific emphasis on those with $\mu < 0''.18 \text{ yr}^{-1}$, the lower cutoff of Luyten's classic proper motion catalog. We used a tightly constrained search of the SuperCOSMOS database and a suite of photometric distance relations for photographic *BRI* and 2MASS *JHK_s* magnitudes to estimate distances to more than fourteen million red dwarf candidates. Here we discuss 29 stars in 26 systems estimated to be within 25 parsecs, all of which have $\mu < 0''.18 \text{ yr}^{-1}$, which we have investigated using milliarcsecond astrometry, *VRI* photometry, and low-resolution spectroscopy. In total, we present the first parallaxes of 20 star systems, nine of which are within 25 parsecs. We have additionally identified eight young M dwarfs, of which two are new members of the nearby young moving groups, and 72 new giants, including two new carbon stars. We also present the entire catalog of 1215 sources we have identified by this means.

Keywords: astrometry — solar neighborhood — stars: distances — stars: low mass — stars: statistics — surveys

1. INTRODUCTION

The Solar Neighborhood is the best laboratory for studying the Galaxy in which we live. The optimal place to make a volume-limited study of stars is nearby, where the very faintest stellar and substellar objects are easiest to detect and measure. Nearby binary systems are excellent targets for dynamical mass determination; they are resolvable with smaller orbits and shorter orbital periods than their more distant counterparts. Planetary-mass objects are brighter and have larger angular separations for the same linear separation when they are closer.

Most surveys to reveal the Sun's nearest neighbors focus on detecting stars exhibiting high proper motions, μ . Such surveys identify two categories of stars — disk stars that are close enough that their modest Galactic orbital motion yields an apparent angular motion above the search threshold, and more distant stars

with much higher intrinsic motions, e.g., subdwarfs and halo stars. This property of large proper motion has served nearby star research well from the very beginning, forming at least part of the decisions of Bessel (1838) and Henderson (1839) to observe 61 Cygni and Alpha Centauri (respectively) for the first parallaxes. These searches have continued on into the present day, encompassing everything from historical efforts like the Luyten Half Second catalog (Luyten 1957, 1979) to recent efforts like LSPM-North (Lépine & Shara 2005) and the Research Consortium On Nearby Stars (RECONS) group's own work (e.g. Henry et al. 2004; Subasavage et al. 2005a,b; Finch et al. 2007; Boyd et al. 2011b,a). These searches have yielded thousands of stars that are candidates for stars within 25 parsecs (pc), the horizon adopted by the Catalog of Nearby Stars (Gliese & Jahreiß 1991) and NStars (Backman et al. 2001) compendia.

Nearly all known nearby stars have high proper motions. An analysis of the current RECONS 10 pc sam-

ple¹ to explore the realm of low μ nearby stars is revealing. Of the 259 systems (not including the Sun) within 10 pc as of 2012 JAN 01, 133 (52%) have $\mu \geq 1.00''\text{yr}^{-1}$, 88 (35%) have $1.00''\text{yr}^{-1} > \mu \geq 0.50''\text{yr}^{-1}$, and 32 (13%) have $0.50''\text{yr}^{-1} > \mu \geq 0.18''\text{yr}^{-1}$. Only two stars, less than 1% of the total sample, have $\mu < 0.18''\text{yr}^{-1}$: GJ 566 AB (spectral type G8V, $V = 4.67$ (Høg et al. 2000), $\mu = 0.169''\text{yr}^{-1}$), and LSPM J0330+5413 (an M dwarf with $V \sim 16$, $\mu = 0.150''\text{yr}^{-1}$, Lépine & Shara 2005).

There are reasons to suspect that a small but significant population of nearby, very low proper motion stars have been overlooked. The limits of the proper motion samples set above are based on historical precedent. In particular, the value of $0.18''\text{yr}^{-1}$ as the lowest interesting proper motion, used by RECONS' other survey samples (e.g. Winters et al. 2017) as its lower limit, comes from the influential surveys of Luyten (Luyten Palomar, Luyten Bruce, Luyten Two Tenths, New Luyten Two Tenths) and Giclas (Southern survey). Those studies were themselves influenced by the work of the Royal Greenwich Observatory, particularly Thackeray (1917) and Dyson (1917), the latter of which suggests that Greenwich set their $0.2''\text{yr}^{-1}$ limit based on calculations that suggested only one-eighth of all nearby stars (<20 pc) should have lower proper motions. Thus, from the outset, it was understood that some population of nearby stars would be overlooked.

In this paper, we present a survey of those very low proper motion stars, along with astrometric, photometric, and spectroscopic follow-up observations for selected high priority stars and other additional targets of interest from the Cerro Tololo Inter-american Observatory Parallax Investigation (CTIOPI) parallax program. In Section 2 we lay out the background work done on these ‘‘TINYMO’’ systems that have $\mu < 0.18''\text{yr}^{-1}$. In Section 3 we discuss the design and methodology of the TINYMO survey itself. In Section 4, we discuss further target characterization, which results in the final catalog of targets presented in Section 5. We then discuss the results of the observational followup of our targets in Section 7, and discuss the implications of the TINYMO survey in detail in Section 6.

2. EXPECTED DISTRIBUTION OF TINYMOS

A few surveys have delved into searches for stars with smaller proper motions, most notably Wroblewski-Torres-Costa (Wroblewski & Torres 1989, and subse-

quent) ($0.15''\text{yr}^{-1}$), the LSPM survey (Lépine & Shara 2005) ($0.15''\text{yr}^{-1}$), the ‘Meet the Cool Neighbors’ group (Reid et al. 2007) (limit $0.11''\text{yr}^{-1}$ northern hemisphere, $0.28''\text{yr}^{-1}$ southern hemisphere), and Deacon & Hambly (2007) ($0.1''\text{yr}^{-1}$), and Deacon et al. (2009) ($0.08''\text{yr}^{-1}$). Apart from the anticipated but currently unreleased Lepine SUPERBLINK catalogs ($0.04''\text{yr}^{-1}$ and larger), no efforts are searching for stars with proper motions smaller than $0.1''\text{yr}^{-1}$, or down to truly zero proper motions. These comprehensive searches have not been done, because without the telltale marker of motion on photographic plates (or more recently, CCD images), the investigator looking for nearby stars is inundated by huge numbers of candidates that come pouring out of automated searches (UCAC, Zacharias et al. 2013; PPMXL, Röser et al. 2011).

2.1. Incompleteness of the 25 parsec sample

How many stars do we expect to find within 25 pc at very low proper motions? For the purposes of this work we have made an estimation, using a simulation of the Solar Neighborhood, accounting for spatial and velocity distributions. The spatial distribution within 25 pc is assumed to be uniform because the volume density of K stars (and hotter) in the RECONS 25 pc sample (Jao et al. in prep) is essentially uniform (Figure 1). The decreasing spatial distribution of M dwarfs is assumed to be the result of luminosity-related incompleteness. Accordingly, we assume the overall stellar density matches that of the nearest 5 pc (52 systems in 5 pc, or $0.099\text{ systems pc}^{-3}$) and expect 6500 systems within 25 pc (Note that Regulus is the sole known B star within 25 parsecs, and not within that 5 pc radius). The velocity distribution of the Solar Neighborhood is modeled according to the spectral type of the stars, as given in Aumer & Binney (2009). The hottest stars have the lowest dispersions around the Local Standard of Rest, and cooler stars have increasingly large velocity dispersions up until the Parenago Discontinuity around $B - V = +0.9$, where the average stellar population has had uniform amounts of disk heating. Additional kinematic parameters for subdwarfs and white dwarfs are sourced from Gizis (1997) and Mihalas & Binney (1981), respectively.

To tie the spherical and velocity distributions together, we used the color distribution of spectral types in the RECONS 25 pc database (together with the assumption that all of the missing star systems would be K, M, L, or T dwarfs with the same velocity dispersion) and generated a cumulative luminosity distribution (Table 1) out of which a random number generator can provide ap-

¹ See Henry et al. (2006) for discussion of the definition of a RECONS 10 pc system, and www.recons.org for updated statistics.

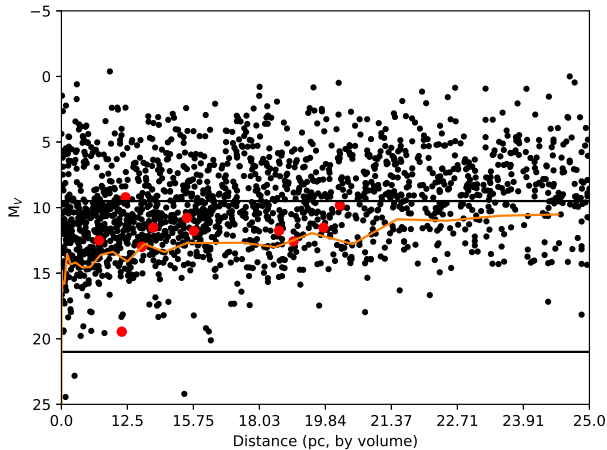


Figure 1. Absolute V magnitude versus Distance for stars within 25 pc, from the RECONS 25 pc database (Jao et al. in prep). The distance is given in equal-volume-elements to properly represent stellar density. The density is essentially uniform for stars brighter than $M_V = 9$, suggesting completeness for A,F,G, and K stars; 90% of stars lie above the orange line, demonstrating completeness decreases at larger distances. Red dots represent the eleven systems within 25 pc with new parallaxes in this paper.

appropriately distributed stars of different spectral types, luminosities, and dispersions. These randomly generated stars were placed in a uniform spatial distribution with a radius of 25 pc. Strömberg’s asymmetric drift equation ($\langle V \rangle = \frac{U^2}{k}$, $k = 74 \pm 5$; Aumer & Binney 2009) was added to the stars, and the UVW velocity of the Sun relative to the local standard of rest ($U=11.10$, $V=12.24$, $W=7.25$ km s $^{-1}$, Schönrich et al. 2010) was subtracted. We then derived the observational properties (RA, DEC, proper motion, radial velocity) from these synthetic stars. The distribution of proper motions, as derived from 10 million synthetic stars, is shown in Figure 2.

As can be seen in Figure 2, the RECONS 25 pc sample is incomplete for all proper motions, but particularly incomplete for proper motions less than $0.5''$ yr $^{-1}$, with peaks in both around $0.3''$ yr $^{-1}$. Overall, 12.4% of all stars within 25 pc should be moving at speeds slower than $0.18''$ yr $^{-1}$, which is in line with other estimates (Reid et al. 2007, for example, find 11%).

There are potential improvements to this simulation: Neither giants nor young stars, nor any of the local kinematic streams (as seen in Skuljan et al. 1999, Nordström et al. 2004) were included in this analysis. An additional possible improvement would be to model stars as bursts of star formation with a cluster mass,

Table 1. Parameters for synthetic 25 pc sample

$V - K_s$	Cum. Frac.	σ_U	σ_V	σ_W	Note
		km s $^{-1}$	km s $^{-1}$	km s $^{-1}$	
-1	0.0000	8	8	5	B systems (Regulus= 1/6375)
0	0.00016	14	9	4.5	A systems (4/408)
1	0.0098	22	14	10	F systems (6/408)
2	0.0245	38	26	20	G systems (20/408)
3	0.0735	37	26	19	K systems (44/408)
3.8	0.1814	37	26	19	M0-3 systems
5	0.3500	37	26	19	M3-5 systems
6	0.5000	37	26	19	M5-7 systems
8	0.7200	37	26	19	M7-9.5 systems
10	0.8100	37	26	19	L,T systems
20	0.91186	37	26	19	Transition ^a
-1	0.91187	177	100	82	Subdwarfs ^b
20	0.92336	177	100	82	Transition ^a
-1	0.92337	50	30	20	White dwarfs ^c
0	0.9500	50	30	20	White dwarfs
2.7	1.0000	50	30	20	White dwarfs

^a These are not real; they are a computational necessity included to separate the “sequences” and prevent interpolation from making many oddly-distributed stars from a continuous function.

^b Gizis (1997)

^c Mihalas & Binney (1981)

NOTE—The cumulative luminosity function (CMF) distribution of stars is in three sequences - main sequence, subdwarfs, and white dwarfs - used to randomly generate a proportional and representative 25 pc sample.

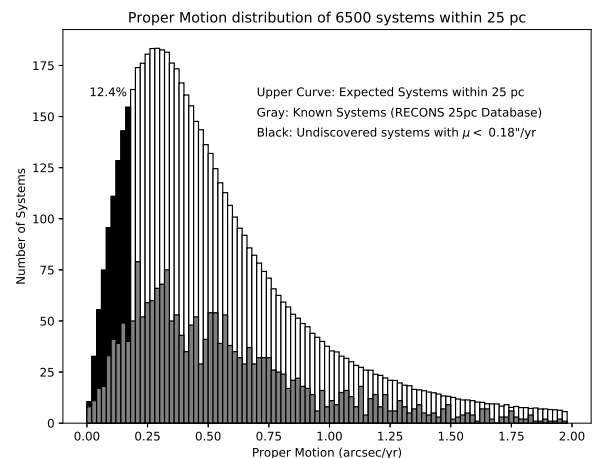


Figure 2. A simulated proper motion distribution using Aumer & Binney (2009), Gizis (1997) and Mihalas & Binney (1981) velocity distributions, and a Cumulative Mass Function (CMF) from RECONS data. The top black and white plotted histogram assumes 6500 star systems within 25 pc, based on the assumption that 52 systems within 5 pc is a representative spatial density. Systems moving slower than $0.18''$ yr $^{-1}$ are noted in black; the gray curve represents actual proper motions from the RECONS 25 pc sample (Jao et al. in preparation).

IMF distribution, and age-associated velocity dispersion.

3. THE TINYMO SURVEY

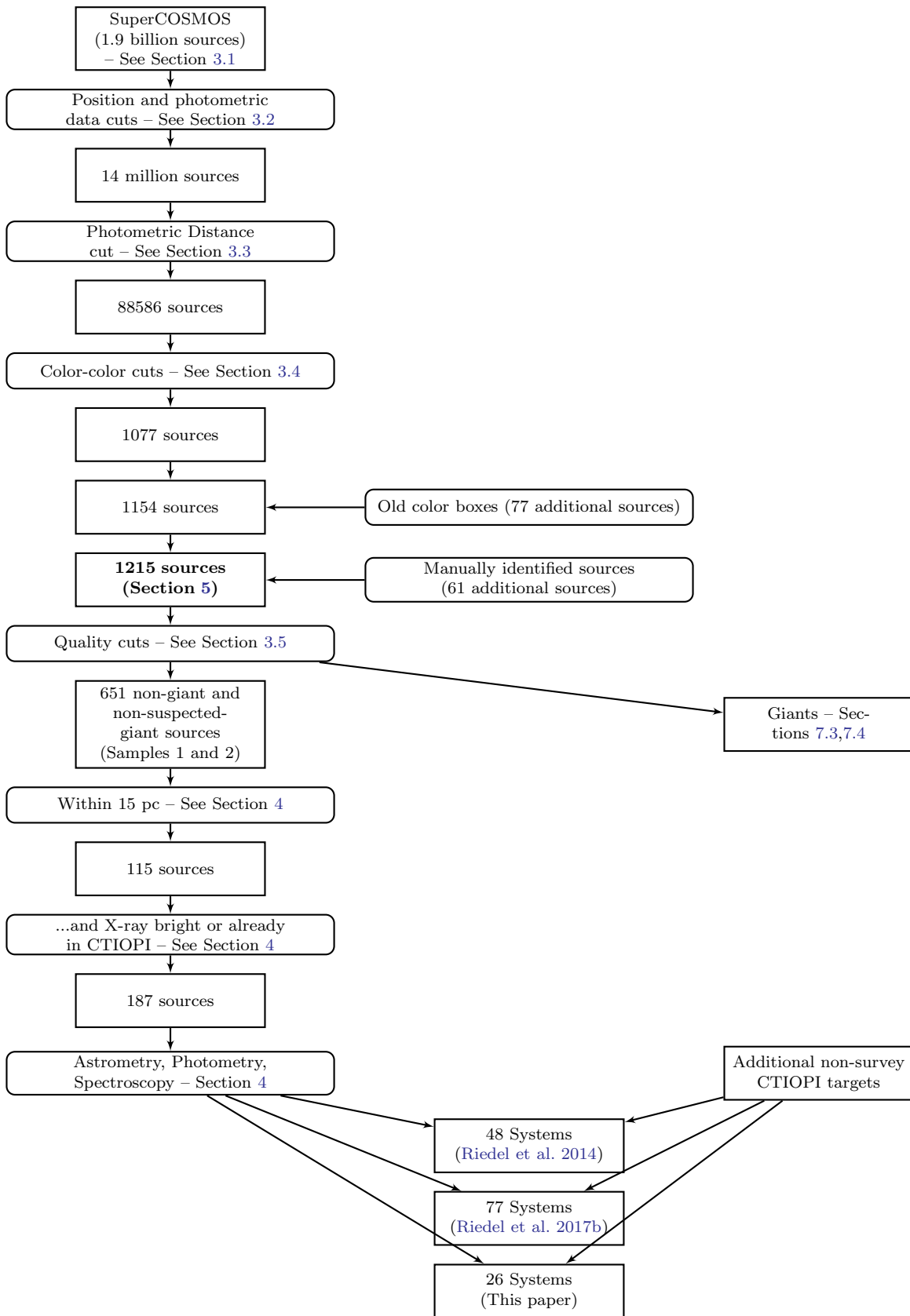
To create a more detailed picture of the Solar Neighborhood, we have carried out a search of the southern sky for stars with tiny proper motions, less than $0.18''\text{yr}^{-1}$, dubbed TINYMO. This is a regime of proper motions that has not been explored in a rigorous way. The discoveries reported here complement previous SuperCOSMOS-RECONS (SCR) searches of the southern sky (Henry et al. 2004; Hambly et al. 2004; Subasavage et al. 2005a,b; Finch et al. 2007; Boyd et al. 2011b,a); in particular, the last three revealed 6007 new proper systems with $0.40''\text{yr}^{-1} > \mu \geq 0.18''\text{yr}^{-1}$ between declinations -90° and -00° , and $R_{59F} = < 18.0$.

Those previous searches used proper motion cuts to identify potential nearby stars, followed by photometric estimates of distance to pick the most promising nearby young objects for astrometric and spectroscopic follow-up through the Cerro Tololo Inter-american Observatory Parallax Investigation (CTIOPI). The search discussed here is almost entirely the opposite of those searches, starting with a rough proper motion limit and

then using photometry to select the promising nearby stars. Photometry is rarely the primary method of identifying nearby stars (one of the rare other examples is Cruz et al. 2007, which identified late-type red dwarfs and brown dwarfs by their extreme colors) because of the enormous contamination of distant giants and other non-nearby sources.

Despite this challenge, a photometric search is the only way to reliably identify genuinely nearby tiny proper motion stars. Even allowing for the practical limitations of proper motion measurements (particularly those of compiled catalogs, which have uncertainties introduced by source/scanning resolution and optical defects), below a certain level (See Section 6.3), even distant background stars have some non-zero proper motion, because they too are in orbit around the Galactic center.

In this paper we estimate distances *en masse* for millions of sources, then target those with the smallest distances for further consideration. The list of selected nearby red dwarf candidates is sequentially winnowed with quality and color cuts until only the most promising targets remain, and these are investigated individually for available data in the literature and targeted in observational programs (See Figure 3).



3.1. *SuperCOSMOS* (1.9 billion sources)

SuperCOSMOS was a machine that scanned glass photographic plates for more than a decade at the

Royal Observatory in Edinburgh (ROE), Scotland. The SuperCOSMOS Science Archive (SSA) database (Hambly et al. 2001b) is built from scans the machine made of primarily Palomar Observatory Sky Survey (POSS) and Science and Engineering Research Council (SERC) sky survey plates. The survey covers the entire sky at four different epochs and in four different passbands, deriving positions, proper motions, and (up to) four-color photometry for 1.9 billion sources. SuperCOSMOS magnitude limits vary by field but are generally equivalent to $B=22$, $R=20$, $I=19$ in the plate photographic magnitude system of (e.g. Bessell 1986). 2MASS JHK_s photometry has been cross-matched to sources where available. SuperCOSMOS is *not* a source of absolute positions or proper motions, though attempts were made to force the mean Galaxy proper motions (field by field) to zero in fields where galaxies were available (Hambly et al. 2001a). The overall reference frame was shifted to ICRS via cross-matching with 2MASS (which is linked to TYCHO-2).

Of interest to TINYMO, the plates were aligned by cross-matching stars out to distances of $6''$ (in a spiral search pattern) between two plates. This matching constraint actually provides a variable *upper* limit on measurable proper motions. For the southern hemisphere where epoch spreads are 30-40 years, the maximum proper motion detectable is around $0.2\text{-}0.3'' \text{ yr}^{-1}$, above which an object would move more than $6''$ in that time. This represents a tradeoff: a few higher proper motion stars – perhaps a hundred thousand out of two billion – will be identified as multiple transient objects. Previous RECONS proper motion searches have been carried out using additional software designed to match up otherwise unmatched sources in the SSA. Other surveys using the SuperCOSMOS Database (and their own special software) include Scholz & Meusinger (2002) (and subsequent), the Liverpool-Edinburgh High Proper Motion Survey (Pokorny et al. 2003), and the Southern Infrared Proper Motion Survey (Deacon et al. 2005).

For the purposes of TINYMO, the main catalog is sufficient, provided we limit ourselves to sources identified on all four plates. The catalog contains proper motions up to $0.3'' \text{ yr}^{-1}$ for sources of interest, except in regions north of $\text{DEC} = -18^\circ$, where far older POSS-I E red plates were used. In those areas, the larger epoch spread means that the highest proper motion that can be reliably extracted from the $6''$ crossmatch is roughly $0.12'' \text{ yr}^{-1}$; it is also incomplete for a 25 square degree region around $\text{RA}=16\text{h}$, $\text{DEC}=-12^\circ$ where POSS-I E field 1038 is missing (and thus no four-color detections are possible).

3.2. SQL Query (14 million sources)

The initial sift of the TINYMO survey was an SQL query, meant to identify meaningful targets in the Southern hemisphere. To avoid overloading the server, the queries were conducted in tiles of RA and DEC. The selection criteria were as follows:

3.2.1. Location Cuts

- Regions in the Southern hemisphere.
- More than 20 degrees from the Galactic Center.
- More than 10 degrees from the Galactic Plane.

These positional cuts were designed to limit the survey to the Southern hemisphere, and remove extremely dense areas (full of highly reddened stars that would contaminate the sample) from consideration. After the fact, additional cuts were made to the extracted data to remove regions near the North Galactic Spur: $15\text{h} \leq \text{RA} \leq 16\text{h}$, $-30 \leq \text{DEC} \leq +00$; $15\text{h} \leq \text{RA} \leq 16\text{h}$, $-60 \leq \text{DEC} \leq -30$; $17\text{h} \leq \text{RA} \leq 18\text{h}$, $-30 \leq \text{DEC} \leq +00$. Within those regions there were as many stars with apparent photometric distances within 25 pc, all most likely giants at far greater distances, as there were in the rest of the sample (see Figure 3). The Large Magellanic Cloud and Small Magellanic Cloud regions were not removed. This cut defines our coverage of 16214 square degrees, or 39.3% of the sky.

3.2.2. Plate Detection Cuts

- Detected on all four plates.

This criterion sets an upper proper motion limit as described above, as well as limits on color – the star could not be so red it did not appear in the B_J plate, which cuts out a number of cool and faint stars. As mentioned earlier, this also cut out a small region of sky (roughly $16\text{h} \leq \text{RA} \leq 16:20$, $-15 \leq \text{DEC} \leq -10$) where there is no R_1 plate.

3.2.3. Quality Cuts

- Internal quality measure > 128 on all plates.
- Ellipticity less than 0.2 on all plates.

These cuts removed a large number of extragalactic sources, unresolved binaries, and spurious sources including plate defects.

3.2.4. Luminosity Cuts

- Brighter than $R_2=16.5$.

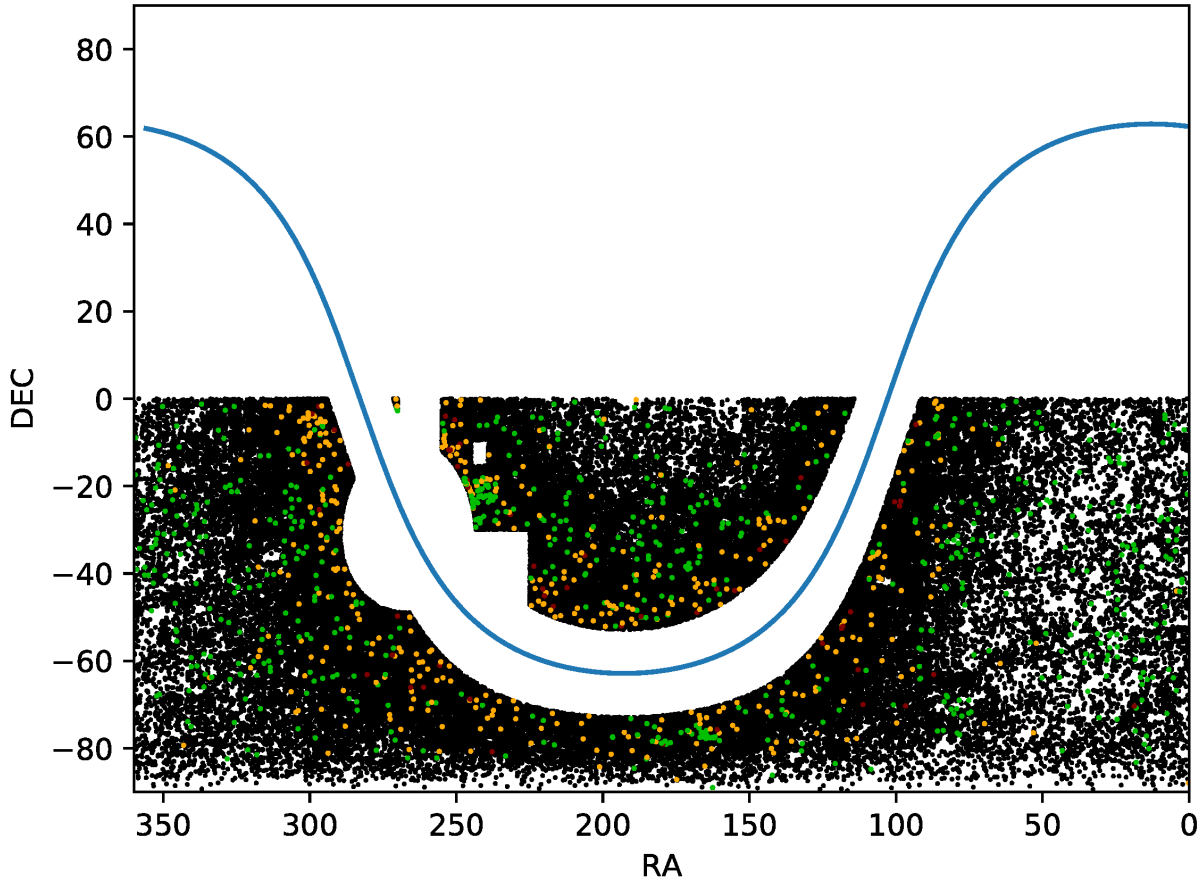


Figure 3. Sky Map of the TINYMO survey extraction centered on RA=0h, DEC=0°, with a 10° band around the Galactic equator and a 20° region around the Galactic Center removed, along with two regions near the North Galactic Spur. The colored points (green = high-probability M dwarfs, yellow = lower probability M dwarfs, red = probable giants) are stars selected by later phases of the survey processing (see Fig 4), demonstrating the crowding of sources around the Galactic bulge. The resulting sky coverage is roughly 16,000 square degrees, or 39.3% of the total sky, and contains just under 14 million targets that satisfy our photometric quality criteria.

The R_2 magnitude limit allows for detection of stars with $B_J=21$ and $B_J - R_2$ colors as red as 4.5 (a brown dwarf), and matches the Giclas surveys (Giclas et al. 1979) as well as previous SCR proper motion surveys, not including Boyd et al. (2011a)

3.2.5. Offset cuts

- Detected in 2MASS within 5'' of the weighted mean plate position.

The mean plate position recorded by SuperCOSMOS is weighted by the positional accuracy of each of the detections; the epoch of this effective plate position is usually around 1985, while the mean epoch of 2MASS is around 2000. Thus, any star moving slower than $\mu < 0.333'' \text{ yr}^{-1}$ (less than $\sim 5''$ motion over 15 years) will

be matched to its 2MASS entry. This, in concert with the four-plate detection requirement, makes the most stringent cut.

The photometric limits chosen influence the kinds of stars we expect to find. The limit of 2MASS is effectively $JHK \approx 15$. SuperCOSMOS contains sources as faint as $B_J = 21$, so with a magnitude cutoff of $R_2 = 16.5$, the limiting magnitudes for M dwarfs are all therefore set by the R_2 filter. The magnitudes of an M0V star ($M_{B_J} = 10$, $B_J - R_2 = 2.3$, $B_J - K = 4.5$) corresponding to our cutoff at $R_2 = 16.5$ are $B_J = 18.8$, $R_2 = 16.5$, and $K = 14.3$. This implies a limiting distance of 630 pc. For an M9.0V star ($M_{B_J} = 20.4$, $B_J - R_2 = 3.0$, $B_J - K = 10.2$) the magnitude limit is $B_J = 19.5$, $R_2 = 16.5$, and $K = 9.3$, which implies a limiting distance of

6.6 pc. Within 25 pc we should be able to detect every M dwarf bluer than $B_J - R_2 = 2.6$ (M7V).

Ultimately, the search identified just short of 14 million stars in the covered 16214 square degree region seen in Figure 3.

3.3. Photometric Sift (88,586 sources)

The next phase of the search for low proper motion nearby stars was the computation of photometric distance estimates (Hambly et al. 2004) for all stars. This method uses the plate BR_2I and 2MASS JHK colors to produce up to 11 distance estimates (out of a total possible 15 colors; $B - R_2$, $J - H$, $J - K$, and $H - K$ do not provide useful discriminants for red dwarfs) that are then combined into a weighted mean with a typical uncertainty of 26%. These color-magnitude relationships, described by fourth-order fits to the main sequence, are only valid for K and M dwarfs, which removes all hotter stars from our consideration. We expect that no stars hotter than K remain undiscovered within 25 pc thanks to the work of *HIPPARCOS*. Of the 14 million point sources from the first step, slightly fewer than 89,000 (see Figure 3) were estimated to be within 25 pc by those relations.

As there are only roughly 6,500 systems expected within 25 pc (Section 2.1), the $\approx 89,000$ figure suggests massive contamination. This is as expected: apart from subdwarfs and (theoretically) stars with unresolved white dwarf companions, contaminants with the colors of main-sequence stars are much brighter objects that will land in a magnitude-limited survey such as ours, and include:

- Giants that mimic main sequence colors or were caught at fortuitous times in their light curves; particularly Mira variables due to their intrinsic luminosity
- Metal-rich stars just beyond 25 pc
- Unresolved multiple stars, where there is extra luminosity and therefore a smaller expected distance.
- Pre-main-sequence stars, where the extra luminosity is due to the enlarged radius of the gravitationally contracting protostar
- Reddened (and extincted) objects in molecular cloud regions
- Redshifted Active Galactic Nuclei

The 11 plate relations were calibrated to colors typical of K and M main sequence stars; if a star has unusual

colors outside the valid color ranges, it is less likely to be a main sequence star. We therefore flagged all objects with fewer than 9 valid distance relations (out of 11 total). It should be noted that this limit is different from that used in other publications in this series, where as few as 7 relations were accepted to accommodate the possibility that a single B_j or R_2 filter magnitude might be erroneous.

3.4. Color-Color cuts (1154 sources)

To identify specifically main sequence stars, we applied a color-color cut, in $J - K$ versus $v - K$ space, where v is an estimated V magnitude formed by taking the average of B and R_2 .

There are, among BR_2IJHK color combinations, two particular colors in which M dwarfs are distinguishable from red giants: $J - H$ and $J - K$ (Figure 4). In these colors (and only these), mid-M dwarfs are bluer than mid-M giants of the same $v - K$ color. This property does not appear in any other combination of colors, including $H - K$, but it shows up when $J - H$ or $J - K$ is plotted against any other color. This behavior is most likely due to gravity-sensitive absorption features in all three bands: The J band feature decreases in strength as gravity increases, and the H and K band features both increase in strength as gravity increases. Allers et al. (2007) identifies a number of potentially gravity-sensitive features that may fit those requirements: VO and TiO weaken with increasing gravity (and are predominantly found in the J band); CO (which dominates in the K band), K I, and Na I all strengthen with increasing gravity. This would explain why dwarfs are bluer in $J - H$ and $J - K$ (increased J flux, decreased H or K flux) and yet there is no effect on $H - K$ (correlated loss of flux). This behavior does not appear in other Johnson/Kron-Cousins/2MASS filter combinations, though R and I are also dominated by TiO; it may have to do with the rate at which the band strengths change.

Plotting the $J - K$ versus $v - K$ combination of colors (Figure 4) demonstrates a region of color-color space where M dwarfs are distinguishable from M giants entirely by photometric colors. To take advantage of that property, we have created four selection regions to separate out the data, as shown in Figure 4 and Table 2.

Region 1: Red Dwarf Candidates

In the Red Dwarf region, the main sequence is clearly separated from the giants, as seen in Figure 4. This is the most reliable region for nearby star detections using our search technique and encompasses spectral types M3.0V through M9.0V. The region has been drawn with a blue cutoff of $v - K = 4.50$ to avoid the broad se-

Table 2. The TINYMO Color Selection Regions

Vertices			
Box	$J - K$	$v - K$	Purpose
1	0.7	4.5	Main Sequence
	0.95	4.5	
	1.2	8.0	
	1.2	10.0	
	0.7	10.0	
2	1.2	8.0	Brown dwarfs
	1.6	10.0	
	1.2	10.0	
3	0.0	10.0	Very red dwarfs
	7.0	10.0	
	7.0	15.0	
	0.0	15.0	
4	4.0	0.0	"Flyers"
	7.0	0.0	
	7.0	9.0	
	4.0	9.0	

quence of giants with bluer $v - K$ seen above the dwarfs, although some nearby stars should be found in this region. Some giants will still bleed into Region 1 near the $J - K = 0.95$, $v - K = 4.50$ corner; the amount of contamination varies from field to field and appears to be related to the Galactic latitude of the region and its particular reddening. The red edge of the sample is cut at $J - K = 1.2$, beyond which the giant and brown dwarf colors overlap.

Region 2: Giants' Tail

The tail of the giant sequence crosses the dwarf sequence in Region 2, but we have retained these targets because one or more may be a very nearby late-type red dwarf or brown dwarf.

Region 3: Very Red Candidates

Region 3 includes extremely red objects ($v - K > 10$) that are also likely giants or highly reddened distant stars, but could be interesting unusually red sources.

Region 4: Flyers

A small group of extremely red sources (called "Flyers") were found to have $v - K = 0-7$ and $J - K = 4-7$. Investigation showed that all were bright targets on the SuperCOSMOS plates, with erroneous matches to 2MASS sources. All checked objects were later determined to be giants falling within the giant locus once their photometry was corrected.

The result of accepting only the objects in these four regions was a reduction of 88,586 candidates to 1077 promising nearby objects. An early selection attempt used different boxes which included 77 stars² not in the

final set of boxes (see Figure 3), which we retain in our final catalog for bookkeeping reasons. This brings the total to 1154 stars.

3.5. Further Quality Cuts

In the fourth and final phase of the winnowing, more quality cuts were made to improve the nearby star recovery rate:

1. visual inspection ("blinking") of SuperCOSMOS plate scans in the Aladin Skyview Desktop applet with the 2MASS Point Source Catalog loaded as an overlay, to ensure detected stars were a.) real objects, b.) moving - proper motions larger than $0.08'' \text{ yr}^{-1}$ were identifiable under visual examination, c.) matched to the proper 2MASS point (mistakes in the 2MASS identification account for the "flyers" mentioned in Section 3.4). At this point, an additional 61 proper motion objects (generally companions) were non-exhaustively identified by eye to bring the total candidate list to 1215 objects.
2. comparisons of the two R band SuperCOSMOS magnitudes for consistency — values differing by more than 1.00 magnitude were likely variable giants and were discarded. This is admittedly imperfect: low-amplitude Mira variables or Miras caught at two similar points in their lightcurve will not be flagged by their $R_1 - R_2$ magnitudes, while stars with bad R_1 or R_2 photometry will be unfairly excluded.
3. elimination of sources with $J - K \geq 2.00$, which are presumed giants or stars with poor JHK magnitudes that corrupt the distance estimates
4. searches of the SIMBAD database to determine whether or not sources are previously documented nearby stars, giants, Mira stars, carbon stars, and/or pulsating or variable stars
5. searches of the Rosat All-Sky Survey (RASS) Bright Source (Voges et al. 1999) and Faint Source (Voges et al. 2000) catalogs for stars with X-ray detections, which are most likely dwarfs or young stars.

We thus arrive at a sample of 651 stars that pass all tests, while the remaining 564 of the 1215 objects were flagged for any number of the above quality reasons.

We developed five classifications for stars based on the above quality cuts, which we use to reclassify the sources identified in the four color boxes defined above, and which we will refer to from this point on:

² None of the 77 objects show signs of being main sequence stars.

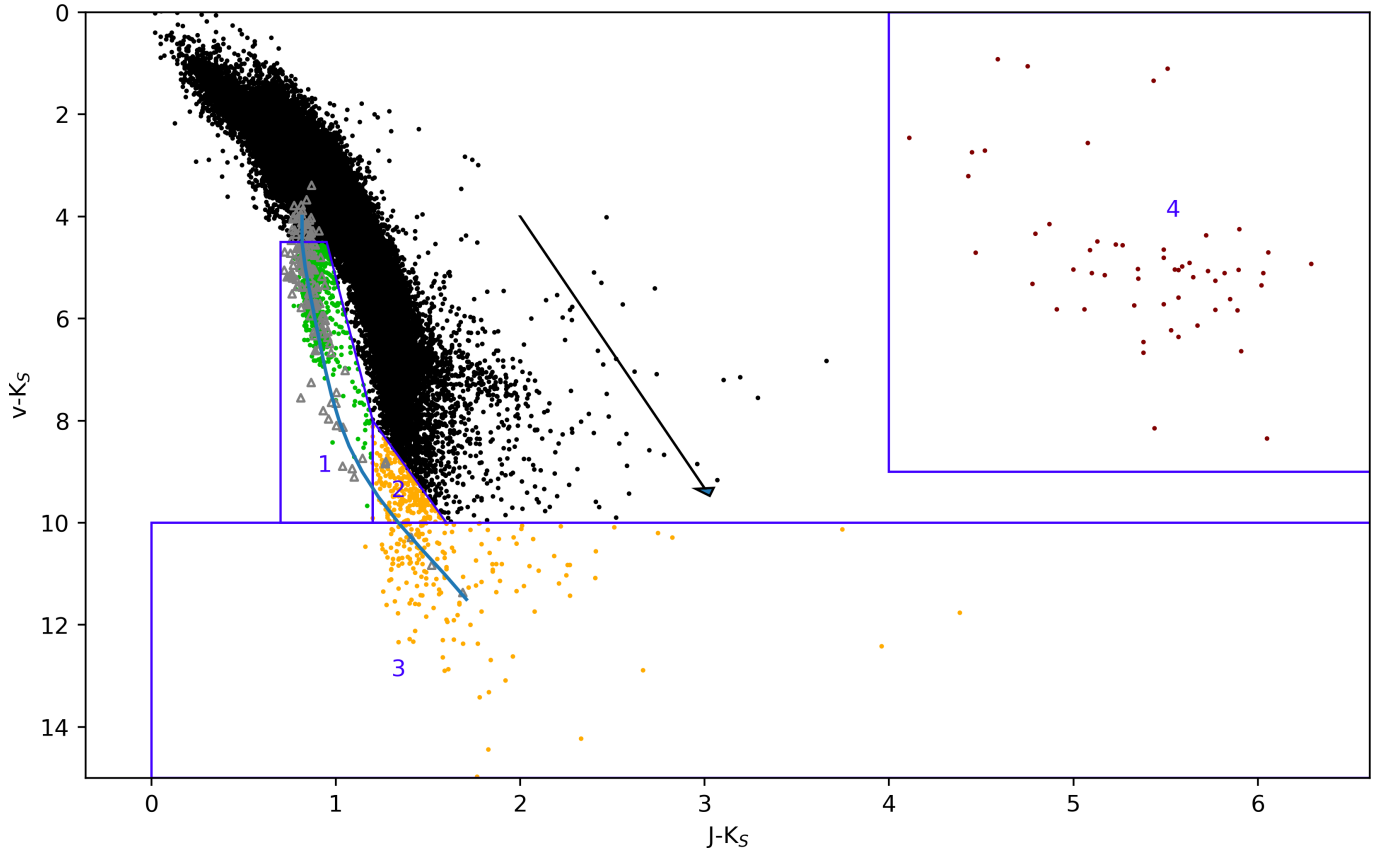


Figure 4. Using the color-color regions shown on this $J - K$ vs $v - K$ diagram, we separate the 88,586 stars in Figure 3 into giants (black), dwarfs (green), and interesting overlap regions (yellow). The curve is a fifth-order fit to the main sequence (as determined by the RECONS 10 pc sample, plotted as gray triangles). The cluster of red points beyond $J - K=4$ (“flyers”) were later revealed to be accidental cross-matches to spurious 2MASS entries. The selection boxes from Table 2 and Section 3.4 are shown here. The appropriate interstellar reddening vector from Fitzpatrick (1999) (assuming $v, J, K_s = \text{Johnson } V, J, K$) is also shown. Colors are the same as on Figure 3.

1. X-ray: Stars that had X-ray counterparts in the RASS-BSC and RASS-FSC catalogs were highest priority, as they were most likely to be nearby dwarfs
2. Good: Stars that passed all quality cuts but did not have X-ray detections
3. Probable: Stars that failed either the $R_1 - R_2$ test, had fewer than 9 valid photometric plate distance relations, or $J - K \geq 2.00$, but were not already known to be giants (as of 2012, Riedel 2012).
4. Giants: Stars known to be giants according to the General Catalog of Variable Stars (Samus et al. 2012, in VizieR as b/GCVS), the Catalog of Galactic Carbon Stars (Alksnis et al. 2001), or SIMBAD.
5. Flyers: Stars from Region 4 of the color-color boxes, the older boxes, or spuriously identified by-eye.

Proper motions from the survey ranged from $0.000'' \text{ yr}^{-1}$ to $0.397'' \text{ yr}^{-1}$; additional targets found by eye were found to be moving as fast as $0.444'' \text{ yr}^{-1}$. Overall, 1016 of the stars found in the survey were moving slower than $0.18'' \text{ yr}^{-1}$

In practice, all but one of the flagged stars in the “Probable” group were revealed to be giants after a literature search or low-resolution spectroscopy (Section 4.3). The one potential nearby star is SCR 1931-1757 (19:31:39.88 -17:57:36.0, $\mu = 0.028 \text{ P.A.} = 188.2^\circ$), a spectroscopically confirmed M2.0Ve star with all 11 valid plate relations and $R_1 - R_2 = -3.03$ (SuperCOSMOS colors are apparently erroneous); its predicted distance was too far (17.67 pc by the average of 12 CCD distance estimates) to earn astrometric follow-up (Section 4).

4. FOLLOW-UP OBSERVATIONS

Given limited observing resources, it was decided to define a higher-priority sample of stars for follow-up. This sample included the 115 tiny proper motion ($< 0.18'' \text{ yr}^{-1}$) candidates with an estimated distance

within 15 pc that had not already been identified as giants in the literature (Regions 1,2, and 3 (if they had more than 9 valid plate relations) of Figure 4), plus all 55 of the targets within 25 pc found to be X-ray bright (Section 4.1). Additional tiny proper motion targets from the survey that were already on the observing programs were folded into our observational list, bringing it to 187 total targets of interest.

For the purposes of providing a larger selection of tiny proper motion objects for analysis in this paper, we added an additional 12 targets from the CTIOPI program that were not found in the TINYMO survey. These additional 12 targets do not appear in the master catalog (Section 5) or discussion thereof, and are marked as such in Tables where they do appear. Their astrometry, photometry, and spectroscopy (where applicable) were obtained in the same way as our survey followup described below.

Analysis of some stars found in the TINYMO sample also appears in Riedel et al. (2014) and Riedel et al. (2017b), and objects with proper motions higher than $0.18'' \text{ yr}^{-1}$ were folded into the study published in Winters et al. (2017).

4.1. Literature Search

There are useful bodies of work in the literature that can be used to further characterize the remaining stars of interest. Apart from SIMBAD, the General Catalog of Variable Stars (Samus et al. 2012, in VizieR as b/GCVS) maintains a list of all known variable stars and can be used to identify Mira variables, Carbon stars, and other semi-regular and irregular giant stars. The Catalog of Galactic Carbon Stars (Alksnis et al. 2001) also furnished some Carbon star identifications. Finally, the entire list was checked against the VizieR versions of the LSPM (Lépine & Shara 2005) and NLTT (Luyten 1979) catalogs to identify previously known proper motion objects. Identifications from these catalogs appear in the catalog (Table 5).

We searched the ROSAT (Voges et al. 1999, 2000) catalog for cross-matches to our objects, as giants are not generally expected to be strong X-ray emitters (I. Song, Priv. Comm.). Voges et al. (1999) defines the 90% limit on detections as being sources within $25''$ of the optical source, with less than 25% uncertainty on the count rate; those guidelines were followed when identifying X-ray sources prioritized for photometry, spectroscopy, and astrometry. Most of these X-ray bright objects were identified as objects of interest by Riaz et al. (2006). Because the ROSAT observations were carried out in the early 1990s, we applied our proper motions to move the targets back to their epoch 1991 positions using the

SuperCOSMOS proper motions before carrying out the X-ray search.

4.2. Photometry

Through the existing CTIOPI program (operating since 1999 on the CTIO 0.9m, Jao et al. 2005; Henry et al. 2006) we have obtained Johnson-Kron-Cousins *VRI* photometry (Jao et al. 2003; Winters et al. 2015) for all 187 targets. Target fields are observed in each filter on photometric nights and then transformed to Johnson-Kron-Cousins *VRI* through the use of standards from Landolt (1992) and Landolt (2007). Stars were observed on at least two nights to check for consistent *VRI* photometry.

The faintest star in our sample is 2MASS 0936-2610B, with $V=19.92$. The brightest star is the unresolved binary GJ 2122AB ($V=9.68$), which is a well-known M1.0V star.

Accurate *VRI* photometric data increase our confidence that the candidate stars are truly nearby dwarfs because (a) the derived distance estimate uncertainties drop from 26% for the plate photometry (and 2MASS) based- BR_2IJHK relations to 15% for the CCD photometry (and 2MASS) based- $VRIJHK$ relations (Henry et al. 2004), and (b) many giants can be eliminated from the candidate pool based on photometric variability revealed by comparing their new CCD Kron-Cousins R magnitudes to existing SuperCOSMOS plate R_1 and R_2 .

The vast majority of this photometry can be found in Table 5. Photometry for all the astrometric targets reported in this paper (including the tiny proper motion systems not found as part of the TINYMO survey) is given in Table 4.2.

Table 3. Photometric Results for 26 Selected Star Systems

Alternate		No. of abs.		σ	No. of rel. No. of		J	H	K_s	spectral	phot	No. of					
Name	Name	V_J	R_{KC}	I_{KC}	Nights	π filter (mag)	Nights	Frames	(2MASS)	(2MASS)	(2MASS)	type	ref ^b	dist	Relations	Notes	
(1)	(2)	(3)	(4)	(5)	(6)	(7)	(8)	(9)	(10)	(11)	(12)	(13)	(14)	(15)	(16)	(17)	(18)
NLT01261	DY Psc	19.88±0.03	17.46±0.07	15.12±0.04	2	I	.0076	7	29	11.99±0.04	11.08±0.02	10.54±0.02	M9.5V	(1)	11.35±2.00	8	
GIC0050	GR 50	13.97±0.05	12.68±0.03	11.00±0.03	2	R	.0130	16	85	9.28±0.02	8.62±0.03	8.35±0.02	M3.0Ve	(2)	11.73±2.04	12	*
2MA0112+1703	GU Psc	14.14±0.04	13.01±0.04	11.61±0.03	2	I	.0167	7	36	10.21±0.02	9.60±0.02	9.35±0.02	M3	(3)	31.24±4.95	12	
2MA0123-6921		19.12±0.19	17.22±0.04	14.91±0.03	2	I	.0139	13	53	12.32±0.02	11.71±0.03	11.32±0.03	M8	(4)	20.42±3.22	12	
SCR0128-1458		13.60±0.04	12.33±0.03	10.67±0.03	3	V	.0099	13	70	9.06±0.02	8.56±0.06	8.20±0.03	M3.0Ve	(2)	12.77±2.00	12	*
BAR161-012	Barta 161 12	13.42±0.03	12.19±0.03	10.57±0.03	2	R	.0510	13	70	8.96±0.02	8.39±0.03	8.08±0.03	M3.0Ve	(2)	12.34±1.95	12	*
SCR0143-0602	RBS 237	13.01±0.03	11.80±0.03	10.25±0.03	2	V	.0368	12	61	8.77±0.02	8.17±0.03	7.91±0.02	M4.0Ve	(2)	13.33±2.05	12	*
SIP0152-6329		15.41±0.05	13.93±0.03	12.01±0.03	2	R	.0141	11	56	10.17±0.02	9.60±0.02	9.26±0.02	M4.5Ve	(2)	13.69±2.15	12	*
SCR0222-6022	RBS 309	13.36±0.05	12.12±0.04	10.52±0.04	3	V	.0408	11	52	8.99±0.02	8.39±0.04	8.10±0.03	M3.0Ve	(2)	13.25±2.03	12	*
2MA0236-5203	EXO 0235.2-5216	12.06±0.03	11.02±0.03	9.75±0.03	2	V	.0397	13	60	8.42±0.02	7.76±0.02	7.50±0.03	M2.5Ve	(2)	15.61±2.88	12	
2MA0254-5108A	GSC 08057-00342	12.08±0.04	11.06±0.04	9.87±0.03	3	V	.0514	14	70	8.67±0.03	8.07±0.06	7.79±0.03	M2.0Ve	(2)	21.45±3.40	12	
2MA0254-5108B		17.56±0.06	15.95±0.09	13.90±0.04	3	V	.0458	14	70	12.07±0.02	11.49±0.02	11.19±0.02			30.48±5.94	12	
SCR0336-2619		16.33±0.04	14.76±0.03	12.72±0.03	2	I	.0117	13	68	10.68±0.02	10.13±0.02	9.76±0.02	M4.5Ve	(2)	14.19±2.21	12	*
RX0413-0139		13.96±0.03	12.66±0.03	10.97±0.03	2	V	.0345	14	58	9.38±0.02	8.76±0.03	8.50±0.02	K5.0Ve	(2)	13.97±2.17	12	
2MA0446-1116AB	RBS 584	12.25±0.05	11.05±0.03	9.57±0.04	2	V	.0162	14	71	8.14±0.02	7.56±0.03	7.29±0.02	M4.9V	(5)	11.07±1.74	12	
HD271076		11.35±0.03	10.33±0.03	9.11±0.03	3	V	.0076	9	40	7.89±0.03	7.32±0.03	7.05±0.02	M2.0V	(2)	15.06±2.32	12	*
SCR0533-4257AB	RBS 661	12.58±0.05	11.27±0.04	9.59±0.03	3	R	.0138	28	141	8.00±0.03	7.40±0.03	7.12±0.03	M4.0VeJ	(2)	7.41±1.15	12	*
LP780-032		12.77±0.03	11.55±0.04	9.99±0.03	3	V	.0111	23	111	8.51±0.02	7.91±0.03	7.65±0.02	M4.0Ve	(2)	11.67±1.80	12	
2MA0936-2610AC		13.12±0.03	11.87±0.03	10.32±0.03	3	V	.0088	9	46	8.86±0.03	8.29±0.05	7.96±0.02	M4.0Ve	(2)	13.57±2.20	12	*
2MA0936-2610B		19.92±0.29	17.46±0.08	14.98±0.02	2	V	12.27±0.02	11.61±0.02	11.21±0.02	17.03±2.73	9	*
SIP1110-3731ABC TWA 3ABC		12.06±0.03	10.82±0.03	9.20±0.03	3	V	...	13	63	7.65±0.02	7.04±0.03	6.77±0.02	M4.0VeJ	(2)	6.99±1.07	12	*
STEPH0164		12.75±0.04	11.59±0.04	10.10±0.03	2	V	.0132	13	55	8.70±0.03	8.07±0.04	7.81±0.03	M3.5Ve	(2)	14.23±2.22	12	*
GJ2122AB	HD 150848	9.68±0.03	8.73±0.03	7.69±0.03	3	V	.0122	40	215	6.57±0.02	5.94±0.03	5.72±0.03	M1.0V	(2)	9.81±1.57	12	
UPM1710-5300AB		11.75±0.03	10.65±0.03	9.31±0.03	2	V	.0149	10	53	8.00±0.03	7.41±0.02	7.16±0.02			13.11±2.03	12	
SIP1809-7613		15.11±0.04	13.62±0.03	11.71±0.03	2	I	.0090	13	67	9.82±0.02	9.28±0.02	8.99±0.02	M4.5Ve	(2)	12.00±1.91	12	*
SCR1816-5844		12.78±0.05	11.62±0.06	10.08±0.04	4	V	.0675	15	62	8.60±0.02	7.96±0.06	7.70±0.02	M3.5Ve	(2)	12.20±1.97	12	*
DEN1956-3207B		13.25±0.03	12.01±0.04	10.45±0.03	2	V	.0196	9	45	8.96±0.03	8.34±0.04	8.11±0.03	M4	(3)	14.18±2.22	12	
DEN1956-3207A	TYC 7443-1102-1	11.54±0.03	10.64±0.04	9.74±0.03	2	V	.0307	9	45	8.71±0.03	8.03±0.04	7.85±0.02			30.21±5.14	12	
BD-13-06424		10.51±0.04	9.58±0.04	8.59±0.03	3	V	.0280	15	77	7.45±0.02	6.77±0.04	6.57±0.02	M0Ve	(6)	14.50±2.67	12	

NOTE—Photometry data collected on the sample. Asterisks in the notes column indicate TINYMO stars identified in the TINYMO survey itself. *VRI* photometry and variability are original, *JHK* is reprinted from the 2MASS Point Source Catalog (Cutri et al. 2003).

^a Astrometric results and relative photometry use new *V* filter data.

^b References: (1) Leggett et al. (2001); (2) This paper; (3) Riaz et al. (2006); (4) Schmidt et al. (2007); (5) Shkolnik et al. (2009); (6) Torres et al. (2006). “J” indicates joint spectral types from unresolved multiples.

4.3. Spectroscopy

For the stars of interest, we obtained high-SNR low resolution long-slit spectroscopy. The primary purpose of this spectroscopy was to identify (and remove) giant stars from our astrometric sample. The data were also intended for spectral typing and used for measuring gravity-sensitive spectral features.

4.3.1. CTIO 1.5m/RCSpec

Most of the spectroscopy were collected on the CTIO/SMARTS 1.5m telescope with the Ritchie-Crétchien spectrograph using the 32/Ia first-order grating (15.13° tilt, 5994Å–9600Å, R=500, OG570 blocking filter), and a 2" slit to maximize the stellar flux. The RC spectrograph uses a relatively old 1200x800 Loral CCD with few bad columns and no backthinning, which minimizes fringing in the red end of the spectrum. Two distinct epochs of observations were conducted, from 2003–2006 for some of the additional CTIOPI targets now being presented here, and from 2009–2011 specifically for the TINYMO survey targets. In both cases, the regular operation was two exposures of the target object, followed by one Neon-Argon (NeAr) lamp exposure for wavelength solution, with one flux standard taken per night.

From 2003–2006, observing was done in person on nine user runs. From 2009–2011, observing was done in SMARTS queue mode. At that time, the 32/Ia setting was no longer a common setup, so for the most part data for TINYMO stars were also collected in single-night blocks. The flux standard was chosen by the queue manager from a small subset of stars, all of which are in IRAF's standard *onedstds*/*ctioneuwal* directory. Spectra were reduced using standard IRAF *onedspec*, *ccdred*, and *ctioslit* packages.

4.3.2. Lowell 1.8m/DeVeny

Additional spectra were gathered at Lowell Observatory's Perkins 1.8m telescope with the DeVeny spectrograph and its 400 g/mm grating tilted at 17 degrees, with the OG570 blocking filter, for coverage from 5800–9200Å at a spectral resolution of roughly R=1500. Spectra were obtained on five runs from 2009 – 2010. Owing to the observatory's northern latitude, only targets north of DEC=−36° were observed from Lowell.

The process of obtaining spectra changed considerably over the course of the project, partly owing to the fact that the DeVeny was not regularly used and rarely in the red end of the spectral range. For the first run (Feb 2009), only one spectrum was taken of each target and standard IRAF flux standard, with Neon-Argon calibration lamp spectra taken at four different times

throughout the night. Subsequent runs (May 2009 and Dec 2009) included lamps taken after each exposure and a large catalog of flatfields, and finally (Mar 2010 and May 2010) flat lamps were taken after every exposure. Spectra were reduced using standard IRAF *onedspec*, *ccdred* and *kpnoslit* packages.

4.3.3. CTIO 4.0m/RCSpec

Ten objects were observed with the CTIO 4.0m RC-Spec on 18 Sep 2008 and 19 Sep 2008, using the KPGLF-1 grating (632 g/mm) and an unknown blocking filter (S. Kafka, private communication). The spectra are higher resolution than our CTIO 1.5m spectra ($\Delta\lambda = 1.90\text{\AA}$, $R \approx 3000$), and cover 4900Å– 8050Å. These spectra do not have the Na I doublet nor Ca II triplet used for gravity and luminosity class detection, but do contain H α and the K I doublet. For some stars this is the only spectrum available.

4.3.4. CFHT/ESPaDONs

LP 780-032 was observed with ESPaDONs on CFHT on 28 Jan 2016. This spectrum is much higher resolution than our CTIO 1.5m spectra and covers 3730Å–10290Å at a resolving power of R=75000. Spectra were processed and flat-fielded through standard methods, and barycentric velocity was removed. LP 780-032 was determined to have a radial velocity of -7 km s^{-1} and rotational velocity of 2 km s^{-1} .

4.4. Astrometry

4.4.1. CTIOPI

TINYMO targets that were spectroscopically identified as dwarfs and were within 15 pc according to *VRIJHK* photometric distance estimates were placed on the CTIOPI astrometric program.

The RECONS group has been conducting the Cerro Tololo Inter-american Observatory Parallax Investigation at the CTIO 0.9m since 1999, until 2003 as an NOAO survey, and 2003–present through the SMARTS Consortium. CTIOPI uses the facility Tek #2 *VRI* filters for observations. For a period of time between 2005 and 2009, the Tek #1 *V* filter was used instead (see [Subasavage et al. 2007](#) for more information). The filter had different astrometric (though not photometric) properties, and all results incorporating data taken in that filter are marked as such in Table 4.2 and Table 4.4.1.

For astrometric observations, target fields are observed usually three times a year within two hours of transit for at least two years in a single filter, chosen out of the *VRI* set to provide the optimal balance between exposure time and brightness of the reference field. Pho-

tometric frames in the appropriate filter that meet image quality and hour angle requirements may be used for astrometry. Data are reduced using the pipeline described in [Jao et al. \(2005\)](#), and as used in all subsequent CTIOPI publications³.

The parallax results (Table 4.4.1) indicate that 15 of the 26 systems presented here are between 25 and 50 pc away, counter to the expectations of the TINYMO selection process, while 11 systems were within the expected 25 parsecs.

4.4.2. FGS

One additional opportunity occurred in 2008 when the Hubble Space Telescope’s data bus developed a fault. As a result, the only available instruments for Cycle 16B were the Fine Guidance Sensors (FGS), which communicate via the telemetry subsystems.

The FGS system on HST can be used as an interferometer, where two of the three onboard Koesters Prisms are used, with one fixed on the target and another scanning around the source to sample the interference pattern, while the third maintains observatory pointing. The output of the interference is two S-shaped curves along orthogonal axes, from which binary stars with separations on the order of tens of milliarcseconds can be resolved by either visually identifying a second overlapping S-curve or, for close-in objects, deviations from the S-curves of a single star.

We took advantage of this opportunity to observe 66 stars from our X-ray bright sample as part of HST program #11943/11944 “Binaries at the Extremes of the H-R Diagram”, PI Douglas Gies. Roughly half of the intended list was observed, and results of newly discovered binaries are mentioned where appropriate in Section 8.

5. THE COMPLETE CATALOG (1215 SOURCES)

The catalog is divided into our five subsamples of descending quality, as described in Section 3.5:

1. Good targets with X-ray detections in the ROSAT All Sky Survey (RASS) – 88 stars, of which 68 have less than $0.18''\text{yr}^{-1}$ (tiny) proper motion.
2. Good targets without X-ray detection – 563 stars, of which 394 have tiny proper motion.
3. Probable giants ($J - K > 1.2, |R_1 - R_2| > 1$) – 222 stars, of which all are tiny proper motion.
4. Known giants (from SIMBAD, the General Catalog of Variable Stars ([Samus et al. 2012](#),

GCVS,)), and the Catalog of Galactic Carbon Stars ([Alksnis et al. 2001](#), CGCS)) – 223 stars, of which all are tiny proper motion.

5. Discarded objects not within 25 pc or not within the color-selection boxes. These were the “flyers” or objects found by eye, but are included for completeness – 119 stars, of which 109 are tiny proper motion.

The final catalog is presented in Table 5. All told, 114 of the stars in the catalog of 1215 targets now have published parallaxes (66 from CTIOPI efforts; 48 from [van Leeuwen 2007](#) and [Gaia Collaboration et al. 2016](#)). 251 stars have new *VRI* photometry, and 229 have new spectral types from red-optical spectra.

6. SURVEY DISCUSSION

6.1. Analysis of the photometric cuts

Figure 5 shows the true $V - K$ colors for all targets actually observed for *VRI* photometry by CTIOPI. This displaces the targets from where they appeared in Figure 4, which was based on the simulated $v - K$ colors. It is apparent from Figure 5 that not all of our “good” (green) targets are actually dwarfs; some of them now lie in the giant locus (which is still drawn with $v - K$ color as in Figure 4). This is unsurprising, as we arrived at our “good” sample by process of elimination, and we did not have the resources to completely vet the sample.

Plotting a histogram of distance estimates from plate *BRI* and 2MASS *JHK* photometry (Figure 6) shows that the original sample was bimodal, with peaks at 25 pc and 1 pc. The giant-sensitive photometric cuts remove most of the stars with predicted distances less than 2 pc. As expected, all potential nearby stars with distances less than 2 parsecs were confirmed with spectroscopy to be giants. All of the 462 nearby low proper motion stars (Categories 1 and 2) can be found among the rest of the sample in the complete Table described in Section 5.

6.2. Completion of TINYMO sample

TINYMO is not complete in terms of proper motions (Figure 7), but this is not surprising as TINYMO uses photometric cuts with no lower proper motion limit, and is not a traditional proper motion survey. TINYMO is probing the range of proper motions more common for giants, which means we also cannot make use of reduced proper motion diagrams that operate under the assumption that lower proper motion objects are farther away; we are specifically looking for nearby stars that move like distant giants, and as Figure 8 shows, the survey contains several such targets.

³ See <http://www.recons.org> for a list of publications

Table 4. Astrometric Results for 26 Selected Star Systems

	R.A.	Decl.							π (Rel)	π (Corr)	π (Abs)	μ	P.A.	V_{tan}	
Name	(J2000)	(J2000)	Filter	N_{sea}	N_{frm}	Coverage ^a	Years	N_{ref}	(mas)	(mas)	(mas)	(mas yr ⁻¹)	(deg)	(km s ⁻¹)	Notes
(1)	(2)	(3)	(4)	(5)	(6)	(7)	(8)	(9)	(10)	(11)	(12)	(13)	(14)	(15)	(16)
NLTT01261	00 24 24.63	-01 58 20.0	I	7s	29	2008.70-2015.82	7.12	6	81.58±2.22	0.85±0.07	82.43±2.22	157.1±0.8	336.4±0.54	9.0	
GIC0050	00 32 53.14	-04 34 07.0	R	7s	85	2007.82-2015.83	8.01	7	51.89±1.05	0.72±0.07	52.61±1.05	167.2±0.5	156.4±0.32	15.1	*
2MA0112+1703	01 12 35.06	+17 03 55.5	I	3s	36	2013.67-2015.96	2.29	6	18.75±2.15	1.85±0.18	20.60±2.16	134.1±2.6	135.1±2.19	30.8	
2MA0123-6921	01 23 11.27	-69 21 38.0	I	7s	53	2008.70-2014.92	6.22	10	22.14±1.37	0.78±0.07	22.92±1.37	87.4±0.7	107.4±0.83	18.1	
SCR0128-1458	01 28 39.53	-14 58 04.2	V	7s	70	2009.93-2015.97	6.04	5	71.84±1.35	3.01±0.23	74.85±1.37	71.9±0.8	226.0±1.30	4.6	*
BAR161-012	01 35 13.94	-07 12 51.8	R	6s	70	2009.94-2014.93	4.99	7	26.11±1.78	1.56±0.27	27.67±1.80	93.3±1.2	114.1±1.38	16.0	*
SCR0143-0602	01 43 45.13	-06 02 40.1	V	6s	61	2009.74-2014.91	5.18	7	49.59±1.48	0.93±0.13	50.52±1.49	47.3±0.9	104.5±1.96	4.4	*
SIP0152-6329	01 52 55.35	-63 29 30.2	R	8s	56	2007.82-2014.93	7.11	7	25.14±1.17	1.39±0.23	26.53±1.19	127.0±0.5	95.7±0.38	22.7	*
SCR0222-6022	02 22 44.17	-60 22 47.6	V	6s	52	2009.75-2014.65	4.90	8	31.76±1.66	0.94±0.13	32.70±1.67	126.2±1.3	98.0±0.92	18.3	*
2MA0236-5203	02 36 51.71	-52 03 03.7	V	6s	63	2009.92-2014.93	5.00	6	25.80±1.24	1.90±0.25	27.70±1.26	80.4±0.8	96.5±0.93	13.8	
2MA0254-5108A	02 54 33.17	-51 08 31.4	V	6c	70	2009.92-2014.91	4.99	6	25.10±1.64	1.95±0.24	27.05±1.66	85.9±1.0	94.6±1.04	15.0	
2MA0254-5108B	02 54 34.77	-51 08 28.8	V	6c	70	2009.92-2014.91	4.99	6	20.52±2.04	1.95±0.25	22.47±2.06	88.2±1.3	92.1±1.20	18.6	
SCR0336-2619	03 36 31.46	-26 19 57.9	I	7s	68	2008.70-2015.08	6.38	9	21.12±1.09	0.68±0.07	21.80±1.09	76.4±0.5	107.9±0.73	16.6	*
RX0413-0139	04 13 26.64	-01 39 21.2	V	6s	58	2009.94-2015.08	5.14	10	35.68±1.90	0.74±0.17	36.42±1.91	127.0±1.5	93.2±0.99	16.5	
2MA0446-1116AB	04 46 51.74	-11 16 47.7	V	5c	71	2011.73-2016.04	4.31	8	70.77±3.41	0.91±0.23	71.68±3.42	149.1±2.1	249.2±1.48	9.9	*
HD271076	05 10 09.69	-72 36 27.9	V ^b	5c	40	2007.81-2011.74	3.93	7	46.73±2.75	2.78±0.46	49.51±2.79	130.7±2.6	80.3±1.81	12.5	*
SCR0533-4257AB	05 33 28.03	-42 57 20.5	R	9c	141	2007.81-2016.05	8.24	9	95.46±1.32	0.98±0.21	96.44±1.34	38.8±0.5	328.8±1.48	1.9	*
LP780-032	06 39 37.41	-21 01 33.3	V ^b	8c	111	2008.70-2016.04	7.34	13	62.26±0.58	1.17±0.11	63.43±0.59	179.2±0.3	294.9±0.17	13.4	*
2MA0936-2610AC	09 36 57.83	-26 10 11.2	V	4c	46	2010.16-2013.38	3.22	9	52.74±1.41	1.01±0.15	53.75±1.42	44.1±1.2	137.7±2.99	3.9	*
SIP1110-3731AC	11 10 27.88	-37 31 52.0	V	6s	63	2009.32-2014.17	4.85	8	28.41±3.97	0.98±0.12	29.39±3.97	91.8±2.5	263.8±2.42	14.8	*
SIP1110-3731B	11 10 27.88	-37 31 52.0	V	6s	46	2009.32-2014.17	4.85	8	30.31±6.82	0.98±0.12	31.29±6.82	114.6±4.4	246.9±4.06	17.4	*
STEPH0164	12 06 22.15	-13 14 56.1	V	5c	55	2010.20-2014.44	4.23	5	31.63±2.36	0.58±0.15	32.21±2.36	113.5±1.7	128.7±1.68	16.7	*
GJ2122AB	16 45 16.97	-38 48 33.3	V ^b	16s	215	2000.58-2016.21	15.63	8	75.69±1.57	1.50±0.50 ^c	77.19±1.64	60.9±0.4	203.8±0.62	3.6	
UPM1710-5300AB	17 10 44.31	-53 00 25.1	V	5c	53	2010.50-2014.27	3.78	10	61.88±2.94	2.67±0.31	64.55±2.96	169.1±2.1	195.9±1.31	12.4	
SIP1809-7613	18 09 06.94	-76 13 23.9	I	5c	67	2010.40-2014.28	3.88	10	36.12±1.50	1.69±0.21	37.81±1.51	143.8±1.2	178.2±0.70	18.0	*
SCR1816-5844	18 16 12.37	-58 44 05.6	V	6c	62	2010.50-2015.29	4.79	9	33.61±1.22	0.86±0.15	34.47±1.23	139.8±0.8	172.8±0.48	19.2	*
DEN1956-3207B	19 56 02.94	-32 07 18.7	V	4s	45	2012.83-2015.68	2.85	6	21.66±1.83	1.09±0.20	22.75±1.84	64.1±1.9	149.3±3.30	13.3	
DEN1956-3207A	19 56 04.38	-32 07 37.7	V	4s	45	2012.83-2015.68	2.85	6	20.93±1.77	1.09±0.20	22.02±1.78	62.9±1.8	148.5±3.24	13.5	
BD-13-06424	23 32 30.87	-12 15 51.4	V	5s	77	2010.73-2015.56	4.83	5	34.19±1.84	0.58±0.05	34.77±1.84	156.5±1.6	108.7±1.04	21.3	

NOTE—Astrometric results derived for the sample. Asterisks in the notes column indicate TINYMO stars identified in the TINYMO survey itself.

^a 'c' indicates continuous coverage, at least two epochs per observing season. 's' indicates scattered observations, with years missing.

^b Astrometric results and relative photometry use new V filter data.

^c Generic correction to absolute parallax was used because the reference starfield appears to be reddened by the nearby dust cloud [DB2002b] G344.85+4.27

6.3. The Limit of Meaningful Proper Motion

TINYMO offers a rough idea of the point at which a proper motion search (even if the proper motions are accurate) will be overwhelmed by giants. This limit (seen in Figure 9) appears to be around $0.035'' \text{ yr}^{-1}$, which is not coincidentally near the lower limit of Lepine’s SUPERBLINK surveys (Lepine & Gaidos 2013), $0.04'' \text{ yr}^{-1}$.

6.4. Why so many young stars?

The TINYMO survey contains a large number of nearby young stars, (55, counting Riedel et al. 2014, Riedel et al. 2017a, and this paper) where they make up perhaps 4% of all stars (Riedel et al. 2017b). There are two primary reasons for this. First, the TINYMO search was carried out using photometric distance estimates, which assumed every star was a single main-sequence star. Pre-main-sequence M dwarfs are brighter and therefore appear closer when estimating distances photometrically, and thus preferentially appear in the

sample. Second, the space velocities of nearby stars are clustered around the local standard of rest (Figure 10) because they are still largely following the paths of the gas clouds from which they formed, and the velocity of the LSR falls below $0.18'' \text{ yr}^{-1}$ beyond 21 parsecs (Figure 11).

The velocity peak at $15\text{-}20 \text{ km s}^{-1}$ is only partially a result of the $0.18'' \text{ yr}^{-1}$ proper motion limit. While it is true that stars moving at $0.18'' \text{ yr}^{-1}$ could have at most 21 km s^{-1} tangential velocities if they were within 25 pc, nearly half of the sample of low proper motion stars were *not* within 25 pc, and thus their V_{tan} was not constrained to 21 km s^{-1} .

6.5. Close passes to the Solar System

Without radial velocities, it is difficult to determine which, if any, of our objects have made close passes to the Solar System. As an educated guess, however, we can take the stars with the lowest V_{tan} velocities as being the most likely to have purely radial mo-

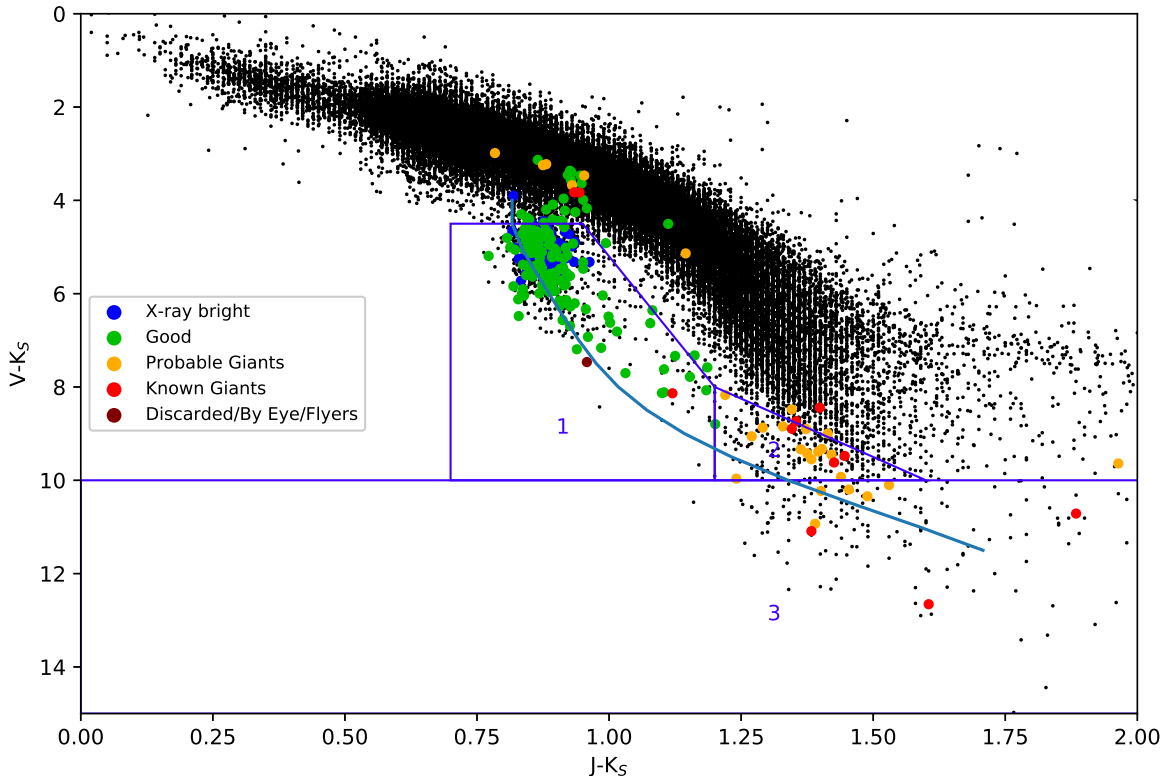


Figure 5. The final state of the TINYMO sample’s subset of stars observed for CCD photometry, plotted on top of the 88,586 stars from the photometric distance cut from Figure 4 (black points still use simulated v - K) for comparison. There has been some vertical shifting in the plotted positions of our photometric sample due to the differences between our simulated v and actual Johnson V . 163 of the stars with CCD photometry are low proper motion ($<0.18'' \text{ yr}^{-1}$), the remaining 103 stars are high proper motion stars observed for other reasons (other CTIOPI targets recovered by TINYMO).

tion. The most obvious contender is SCR 0613-2742AB, the β Pic member published in Malo et al. (2013) and Riedel et al. (2014). It does have a published radial velocity, ($+22.54 \pm 1.16 \text{ km s}^{-1}$, Riedel et al. 2014), which places its closest approach to the Solar System (using an epicyclic approximation to Galactic motion, Riedel et al. 2017b) as 1.2 Myr ago, at a distance of 6.1 pc. SCR 0533-4257 may be a more likely target, but without a radial velocity it is hard to identify.

Boylev (2010) lists no less than six stars predicted (via a more rigorous Galactic potential analysis) to come closer than SCR 0613-2742AB: GJ 710 (0.21 pc), GJ 551=Proxima Centauri (0.89 pc), GJ 559A= α Centauri A (0.91 pc), GJ 559B= α Centauri B (0.91 pc), GJ 445 (1.06 pc), and GJ 699=Barnard’s Star (1.15 pc). Of those stars, the most remarkable is GJ 710, with proper motion vectors ($\mu_{RA} = 1.15 \pm 1.66 \text{ mas yr}^{-1}$, $\mu_{DEC} = 1.99 \pm 1.22 \text{ mas yr}^{-1}$), far smaller than any stars in the TINYMO survey.

7. RESULTS

7.1. Nearby Stars

Although the majority of the stars followed up by the TINYMO survey were not within the 15 pc limit for which they were selected, there are 11 new stars within 25 pc in this sample. Most notable among them are SCR 0533-4257AB, a binary almost within 10 pc of the Sun, and HD 271076, which sits in front of the Large Magellanic Cloud and was at one time mistaken for a supergiant member of that satellite galaxy. More details of these two stars as well as other highlighted nearby stars are given in Section 8.

7.2. Spectral types

Initial classification was done by eye using the techniques from Henry et al. (2002), Kirkpatrick et al. (1991), Boeshaar (1976), and Keenan & McNeil (1976), which solely focused on identifying dwarfs and giants by Na I, Ca II and K I line features. Many giants

Table 5. TINYMO Catalog Headers

Number	Column	Unit
1	Sample Type ^a	
2	Name	
CTIOPI Astrometry		
3	RA	h:m:s
4	DEC	d:m:s
5	pm	arcsec
6	P.A.	deg
7	pi	mas
8	e_pi	mas
9	r_pi	
SuperCOSMOS photometry		
10	B _j	mag
11	R1	mag
12	R2	mag
13	I _{59F}	mag
14	Blend	
CTIOPI photometry		
15	V	mag
16	V Blend	
17	e_V	mag
18	R	mag
19	R Blend	
20	e_R	mag
21	I	mag
22	I Blend	
23	e_I	mag
24	n_phot	
2MASS photometry		
25	J	mag
26	J Blend	
27	e_J	mag
28	H	mag
29	H Blend	
30	e_H	mag
31	K	mag
32	K Blend	
33	e_K	mag
Spectra		
34	SpType	
35	SpType Ref	
36	ewHa	Å
37	NaI Index	
38	ewKI7699	Å
39	ewNaI	Å
Distance Estimates		
40	plate relations	
41	plate distance	pc
42	e_plate distance	pc
43	CCD relations	
44	CCD distance	pc
45	e_CCD distance	pc
HR Diagram Values		
46	M _v	mag
47	V-K	mag
48	v-K	mag
49	J-K	mag
50	R1-R2	mag
ROSAT X-ray Data		
51	X-ray flux	cnts sec ⁻¹
52	X-ray flux blend	
53	e_X ray flux	cnts sec ⁻¹
54	HR1 Hardness Ratio	
55	HR1 blend	

NOTE—The full catalog is available electronically.

^a The Samples referred to are 1) X-ray bright stars, 2) Good stars, 3) Very Red/Probable Giants, 4) Known giants, 5) Discarded objects, as per Section 5

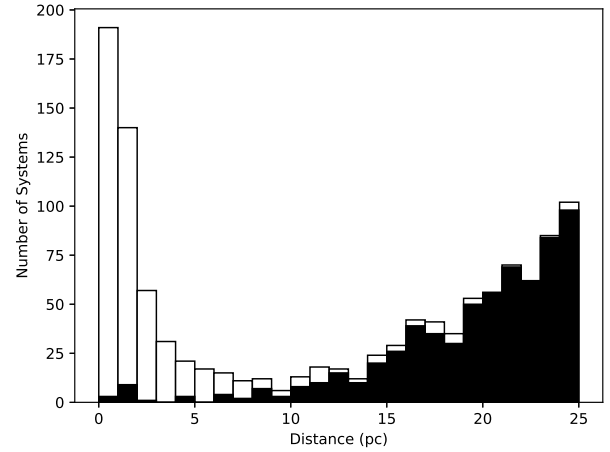


Figure 6. Plate photometric distances for (white) the entire sample of 1215 objects (including later additions found by eye) and (black) the X-ray bright and good candidate samples. The trend of photometric distances is clearly bimodal, although applying our additional photometric cuts has weeded out an immense number of giants that only appeared to be nearby.

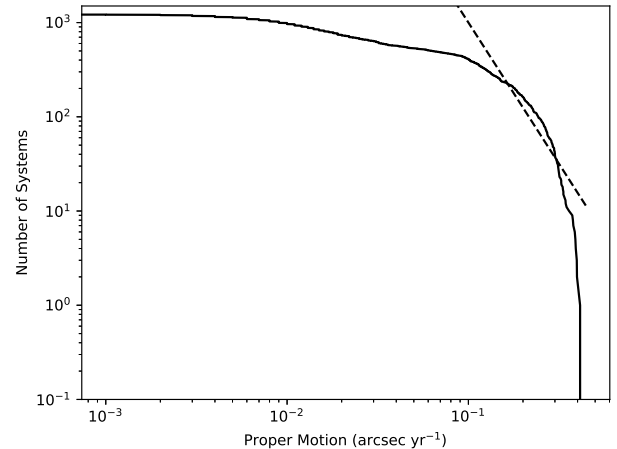


Figure 7. A diagram of the completeness of stars, as in Figure 1 of Lépine et al. (2005). The μ^{-3} curve (dotted line) follows from the assumption that the number density of stars varies as $n \propto d^3$, and proper motion varies as $\mu \propto d^{-1}$. The TINYMO sample is not complete for its proper motions.

were identified this way, as well as two carbon stars. Stars confirmed as dwarfs were placed on the CTIOPI astrometric observing program.

Spectral types (given in Table 4.2) were determined using the MATCHSTAR code (Riedel et al. 2014), a template matching code which operates by comparing input red optical spectra to a series of spectral stan-

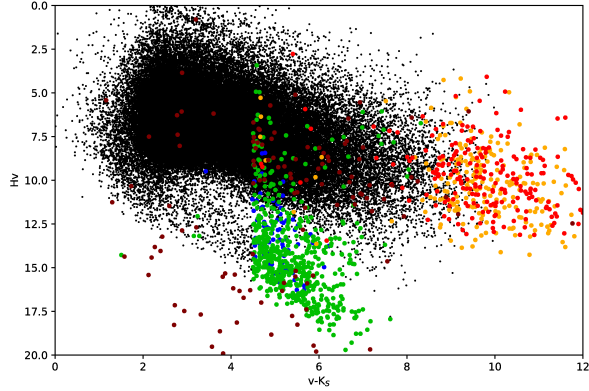


Figure 8. Reduced Proper Motion diagram for the TINYMO sample, where the subsamples are colorized in the same manner as Figure 5. Reduced Proper Motion (H) is $H - v = 5 \log(\frac{1}{\mu}) - 5$ (i.e., μ replaces π in the distance modulus equation). As can be seen above, there are clearly two loci, one (top) for giants, and one (bottom) for dwarfs; while most of the green/blue “good” sample of stars obey those trends, there are clearly green/blue “good” stars in the giant locus.

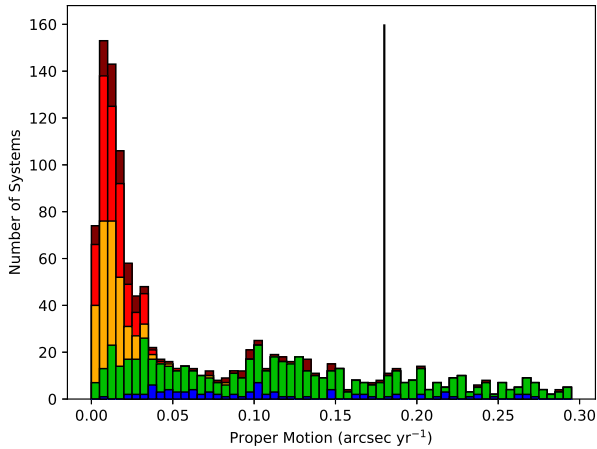


Figure 9. Proper motions of the entire survey (including all higher-proper-motion stars discovered within), in $0.005'' \text{ yr}^{-1}$ bins. Color follows Figure 5. Below $0.035'' \text{ yr}^{-1}$, the sample is dominated by giants and suspected giants, while above that, it is dominated by X-ray bright and regular stars. The vertical line is at $0.18'' \text{ yr}^{-1}$, and divides TINYMO and higher proper motion targets found in the survey.

standard star spectra (Kirkpatrick et al. 1991, Henry et al. 1994). The code selects the portions of the spectrum held in common between both target and standard star, masks out the atmospheric bands and $H\alpha$ emission line, divides the spectra by the templates, and takes the lowest standard deviation of a match as the correct spec-

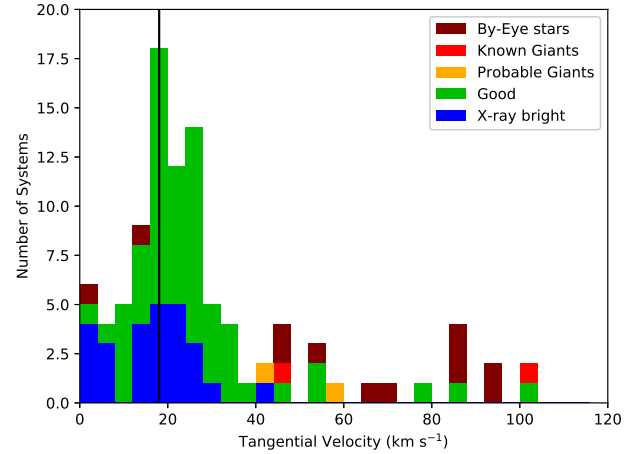


Figure 10. The tangential velocity distribution for the stars in the TINYMO sample with parallaxes. Despite having no overall constraint on V_{tan} , the distribution peaks at 15-20 km s^{-1} , near the Local Standard of Rest (vertical black line).

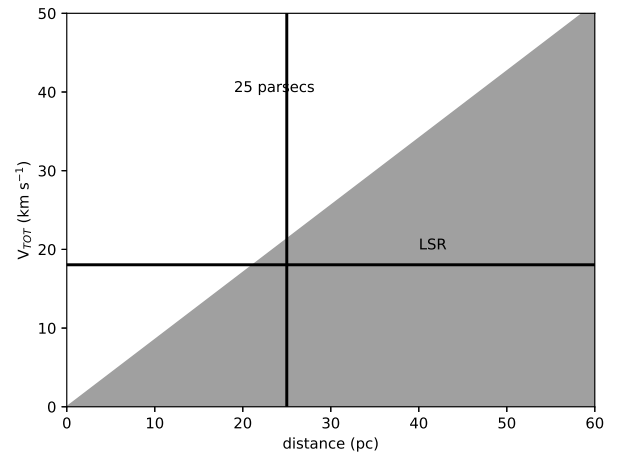


Figure 11. Objects whose distance and tangential velocity fall within the white region will move more than $0.18'' \text{ yr}^{-1}$; stars within the gray region will have lower proper motions. Stars moving at the velocity of the Local Standard of Rest (LSR, 18 km s^{-1}) move slower than $0.18'' \text{ yr}^{-1}$ if they are more than 21.1 pc away.

tral type. In this way, the code is able to type K0-K9 stars in whole types and M0.0-M9.0 in half types with a 0.5 spectral type uncertainty, as determined from fitting spectra of stars taken on different dates and with different instruments.

The code also measures, through simple numerical integration, the $H\alpha$ line equivalent width at 6563\AA , the K I doublet line at 7699\AA (the 7665\AA line is masked out as part of the atmospheric A band), and the Lyo et al.

(2004) NaI 8200Å doublet index. Emission is reported as negative equivalent widths.

7.3. They Might Be Giants

Table 7.3 contains a list of the new giants (confirmed by spectroscopy) discovered in the TINYMO search, a list distinct from the stars described in Table 4.2 and Table 4.4.1. The spectral types given in the table were assigned by matching to M dwarf spectra, and identified as giants by Na I index measures of less than 1.02. Accordingly, not much stock should be placed in the actual spectral types of the giants in Table 7.3, as M dwarf types do not correspond directly to giant or supergiant classifications; we also do not provide luminosity classes. The H α emission (denoted by “e” in Table 7.3) reported for three stars does appear to be genuine. Samus et al. (2012) mentions “characteristic late-type emission spectra” in its description of Mira variables, which implies this is a known phenomenon in at least Mira-type giants.

This sample contains thirteen new large-amplitude photometric variables (denoted by “var” in Table 7.3) based on either much larger than typical uncertainties on their CCD photometry (> 0.1 mag mean uncertainty, which matches that of known Miras observed by CTIOPI), or > 1 mag discrepancy between their R magnitudes (SuperCOSMOS and our CCD photometry). These may be Mira variables, but we lack sufficient evidence of periodicity or the required 2.5 magnitude amplitude for the formal definition of Miras. Photometry and other details for these stars can be found in Table 5.

Table 6. New Giants and Supergiants in the TINYMO sample

Name	RA	DEC	SpType ^a
(1)	(2)	(3)	(4)
HD270965	05 00 40.38	-71 57 52.9	K7.0var ^b
SCR0659-5954	06 59 10.94	-59 54 58.6	M6.5var,e ^c
SCR0703-3507	07 03 49.64	-35 07 44.3	M6.5
SCR0705-3534	07 05 47.36	-35 34 25.8	M6.5
SCR0711-3600	07 11 03.53	-36 00 59.7	CARBON
SCR0747-5412	07 47 14.27	-54 12 02.5	CARBON
SCR0747-6355	07 47 25.60	-63 55 42.3	K7.0
SCR0749-6502	07 49 05.69	-65 02 40.0	K8.0
SCR0753-5150	07 53 24.57	-51 50 22.0	M9.0
SCR0753-6641	07 53 49.77	-66 41 38.3	K9.0
SCR0805-0743	08 05 52.81	-07 43 05.7	M9.0
STEPH0097	08 14 24.82	-13 02 22.6	M6.5
SCR0833-6107	08 33 27.67	-61 07 58.4	M4.5var ^b
SCR0857-6734	08 57 38.21	-67 34 10.5	M5.0
IRA08583-2531	09 00 32.06	-25 43 14.1	M8.0
SCR0902-7823	09 02 35.97	-78 23 14.7	M7.5
SCR0910-7214	09 10 57.71	-72 14 52.9	M5.0
SCR0927-8105	09 27 04.18	-81 05 00.7	M4.5var,e ^c
SCR0932-2806	09 32 03.32	-28 06 27.0	M9.0

Table 6 continued

Table 6 (continued)

Name	RA	DEC	SpType ^a
(1)	(2)	(3)	(4)
SCR0938-3748	09 38 20.24	-37 48 44.6	M6.5
SCR0945-3430	09 45 43.54	-34 30 18.1	M4.5var ^c
SCR1044-7543	10 44 06.77	-75 43 42.2	M2.5
SCR1044-4330	10 44 40.73	-43 30 44.2	M6.5
SCR1048-7739	10 48 26.67	-77 39 19.1	M0.0
SCR1058-4218	10 58 44.39	-42 18 12.3	M6.5
SCR1111-4856	11 11 28.25	-48 56 14.3	M2.5
SCR1138-4338	11 38 13.34	-43 38 04.6	M9.0
SCR1228-4949	12 28 06.16	-49 49 34.5	M5.0
STEPH0172	12 34 41.61	-00 14 14.1	M9.0
SCR1306-4745	13 06 42.81	-47 45 25.7	M6.5var ^c
SCR1316-5206	13 16 42.18	-52 06 38.3	M6.5
SCR1317-4643	13 17 56.50	-46 43 54.0	M9.0var ^d
SCR1321-4913	13 21 31.72	-49 13 09.6	M7.5
SCR1349-7417	13 49 16.98	-74 17 15.4	M9.0
SCR1358-4910	13 58 43.58	-49 10 52.0	M7.0
SCR1408-3506	14 08 36.51	-35 06 02.3	M6.5
SCR1424-4427	14 24 36.78	-44 27 05.6	M7.5
SCR1427-4731	14 27 43.90	-47 31 13.2	M4.0
SCR1431-4823	14 31 28.46	-48 23 12.1	M7.0
SCR1439-4506	14 39 33.26	-45 06 42.3	M4.5
SCR1440-7837	14 40 37.43	-78 37 11.4	K8.0
SCR1458-4102	14 58 23.80	-41 02 27.9	M7.0var ^e
CD-81-00572	15 32 44.68	-81 43 53.0	K8.0
SCR1534-7237	15 34 02.51	-72 37 11.1	M6.5
SCR1544-1805	15 44 44.97	-18 05 07.1	M9.0
SCR1551-8047	15 51 10.25	-80 47 51.5	M3.0
STEPH0257	15 58 20.04	-06 03 37.4	M7.0
SCR1604-7009	16 04 23.14	-70 09 03.1	M5.0
SCR1612-6858	16 12 30.09	-68 58 52.7	M6.5
SCR1621-6843	16 21 18.53	-68 43 58.4	M6.5
SCR1647-6436	16 47 48.35	-64 36 43.6	M5.0
SCR1654-0055	16 54 08.17	-00 55 04.9	M9.0
SCR1658-6350	16 58 12.94	-63 50 49.3	M7.5
SCR1706-6426	17 06 39.02	-64 26 23.3	M7.5var ^c
SCR1719-6151	17 19 09.42	-61 51 55.7	M9.0
SCR1738-6844	17 38 14.51	-68 44 52.8	M5.0var ^c
SCR1743-4959	17 43 35.28	-49 59 10.6	M9.0
SCR1803-7807	18 03 30.88	-78 07 21.7	M4.5
SCR1807-5839	18 07 22.90	-58 39 59.9	M4.5
SCR1919-2943	19 19 23.11	-29 43 15.0	M9.0
CD-35-13495	19 27 08.18	-35 15 09.6	M7.5
SCR1943-0138	19 43 43.06	-01 38 31.6	M6.5
SCR1944-3414	19 44 45.52	-34 14 41.2	M9.0
CD-45-13476	19 53 08.97	-45 15 15.5	M7.5
SCR1959-1639	19 59 35.79	-16 39 20.3	M8.0
SCR2000-0837	20 00 58.33	-08 37 27.5	M9.0e
SCR2024-2500	20 24 15.40	-25 00 56.8	M6.5
SCR2038-0409	20 38 45.49	-04 09 27.0	M5.0
SCR2107-5734	21 07 58.01	-57 34 17.5	M7.0var ^d
SCR2138-4308	21 38 15.11	-43 08 40.6	M6.5var ^f
CD-24-17228	22 34 29.69	-24 15 17.7	M6.5
SCR2305-3054	23 05 14.88	-30 54 37.1	M5.0var ^g

^a Spectral Types derived from comparisons to dwarfs, and may not be accurate.

^c Variable status inferred from >1 magnitude R_2 and R_{kc} magnitude mismatch. ^e Variable status inferred from >1 magnitude R_1 and R_2 plate magnitude mismatch. ^d Variable status inferred from >1 magnitude R_1 and R_{kc} magnitude mismatch. ^e R_{kc} filter variability 0.18 mag. ^f R_{kc} filter variability 0.31 mag. ^g R_{kc} filter variability 0.54 mag.

7.4. Carbon Stars

Three carbon stars were observed during data collection. One, IY Hya, was observed as a comparison object; the other two are new discoveries. Figure 12

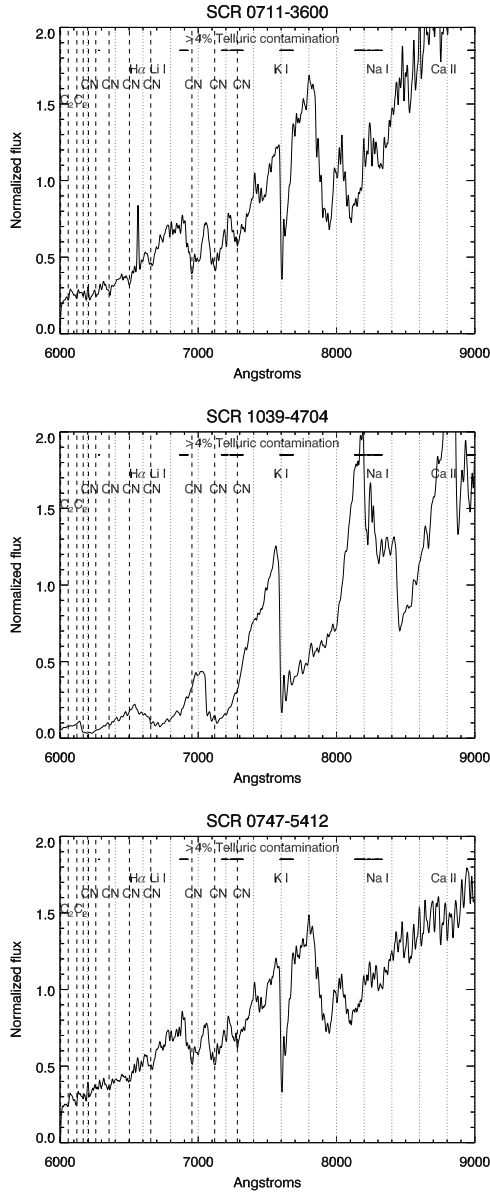


Figure 12. CTIO 1.5m spectra of the two new carbon stars, SCR 0711-3600 (top), and SCR 0747-5412 (bottom), both from 2009 SEP 16, along with the approximately M7.5III giant SCR 1039-4704 (middle, from 2010 Dec 20) for comparison. The spectrum of a carbon star is unlike an M dwarf or M giant, and contains unusual concentrations of carbon molecules (here, CN bands known as Swan bands) rather than the typical TiO or VO bands of an M dwarf (compare, for instance, the spectral morphology at 7100Å).

shows the spectra of the new stars and a normal M giant for comparison. Based on comparisons with spectra in [Turnshek et al. \(1985\)](#), they appear to be genuine C-type stars with CN bands at 6900, 7100, 7500, 7900, and 8100Å.

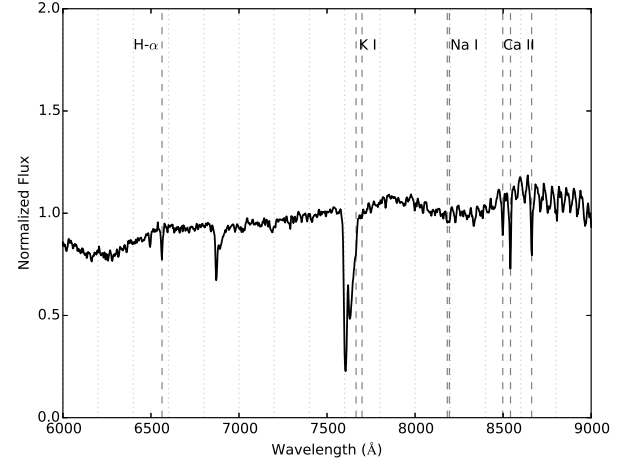


Figure 13. CTIO 1.5m spectrum of the reddened star BD-19-04371 on 17 Sep 2010. The star is an apparent member of the Upper Scorpius star forming region. Its colors are of an M dwarf, but it is missing the strong TiO bands of M dwarfs.

7.5. Reddened Stars

Several reddened stars were picked up in TINYM0; these mostly appear to be members of various subsets of the Sco-Cen star forming region. BD-19 04371 (16:26:23.37 -19:31:35.7), SCR 1627-1925 (16:27:14.03 -19:25:46.7), and SCR 1627-1924 (16:27:14.79 -19:24:16.3) are all in the region of the sky with the Upper Scorpius star forming region, and all appear to be reddened stars of hotter spectral types (Figure 13).

A few other stars were pre-identified in SIMBAD as members of the Chamæleontis I dark cloud (CHXR11, 11:03:11.61 -77:21:04.2), or ϵ Chamæleontis association. The only truly unusual set of reddened potential nearby stars were a quartet of reddened objects:

- CD-58 07828 20:39:19.56 -58:02:29.4 $\mu = 0.036$ @ 099.3^o yr^{-1}
- CD-61 06505 20:54:02.76 -61:28:25.4 $\mu = 0.002$ @ 010.5^o yr^{-1}
- SCR 2055-6001 20:55:43.94 -60:01:46.1 $\mu = 0.018$ @ 010.4^o yr^{-1}
- SCR 2116-5825 21:16:44.72 -58:25:25.2 $\mu = 0.014$ @ 218.1^o yr^{-1}

There is no known cloud in this location (as per WEBDA), which is at a high Galactic latitude. It may be that these stars are truly unrelated (their proper motion vectors from SuperCOSMOS appear different, but statistically consistent with $\mu = 0$) and all just happen

to be reddened, but they are the only concentration of reddened objects that cannot be immediately explained.

7.6. *New Young Stars*

Table 7. Youth Criteria of Parallax targets

Name	LACEwING	Kinematic	H- α	Na Index	KI EW	Youth	Note
(1)	Group	Prob. (%)	RV (km s ⁻¹)	\AA	idx.	\AA	Flags ^a
(1)	(2)	(3)	(4)	(5)	(6)	(7)	(8)
(1)	(2)	(3)	(4)	(5)	(6)	(7)	(8)
NLTT 1261	(None)						...
GIC 50	(None)			-1.83	1.22	2.05	*
2MA 0112+1703	AB Dor	73	-1.4 \pm 1.9				...
2MA 0123-6921	Tuc-Hor	85	+9.9 \pm 3.4				...
SCR 0128-1458	(None)			-3.49	1.22	2.23	*
BAR 161-012	(None)			-10.51	1.15	1.43	h N K *
SCR 0143-0602	(None)			-5.32	1.20	1.76	*
SIPS 0152-6329	Tuc-Hor	80	+10.4 \pm 3.4	-9.72	1.19	2.52	N *
SCR 0222-6022	Tuc-Hor	88	+11.5 \pm 3.3	-11.56	1.18	1.07	h N K *
2MA 0236-5203	Tuc-Hor	86	+11.7 \pm 3.1	-5.53	1.09	0.54	N
2MA 0254-5108A	Tuc-Hor	33	+12.7 \pm 3.1	-2.08	1.09	0.66	
2MA 0254-5108B	Tuc-Hor	63	+12.6 \pm 3.1				...
SCR 0336-2619	Tuc-Hor	67	+13.5 \pm 2.6	-10.19	1.25	2.47	h N K *
RX 0413-0139	(None)			-10.54	1.18	1.11	h N K
2MA 0446-1116AB	(None)						...
HD 271076	(None)			+0.20	1.11	0.82	*
SCR 0533-4257AB	(None)			-4.63	1.20	1.95	*
LP 780-032	Argus	38	+23.8 \pm 1.8	-0.26	1.21	1.69	
2MA 0936-2610AC	(None)			-2.36	1.26	2.45	*
SIPS 1110-3731AC	TW Hya	72	+12.7 \pm 2.2	-9.21	1.10	0.51	N K *
SIPS 1110-3731B	TW Hya	62	+12.7 \pm 2.2	-9.21	1.10	0.51	N K *
STEPH 164	(None)			-4.25	1.15	1.38	*
GJ 2122AB	(None)			+0.28	1.08	0.82	
UPM 1710-5300AB	(None)						...
SIPS 1809-7613	β Pic	31	+6.4 \pm 2.6	-8.31	1.17	1.98	N K *
SCR 1816-5844	Argus	69	-13.0 \pm 1.9	-6.50	1.15	1.09	N *
DEN 1956-3207B	(None)						...
DEN 1956-3207A	(None)						...
BD-13 6424	β Pic	30	+0.9 \pm 1.6				...

NOTE—Youth properties are of stars in Table 4.2 and Table 4.4.1.

^aYouth flags are: “h”: H- α stronger than -10\AA ; “N”: Low surface gravity by sodium index; “K”: Low surface gravity by potassium EW.

A substantial number of targets found in the TINYMO survey were found to be young (Figure 14). In red spectra (6000 \AA – 9000 \AA) there are three useful spectroscopic features that distinguish dwarfs from giants. Ca II is strong in giants and weak in dwarfs; Na I and K I are

weak in giants and strong in dwarfs; the general principle, as outlined in Allers et al. (2007), is that neutral alkali species are stronger in dwarfs, while singly-ionized species are stronger in giants. The Ca II triplet is almost completely absent in mid-M dwarfs, but prominent in

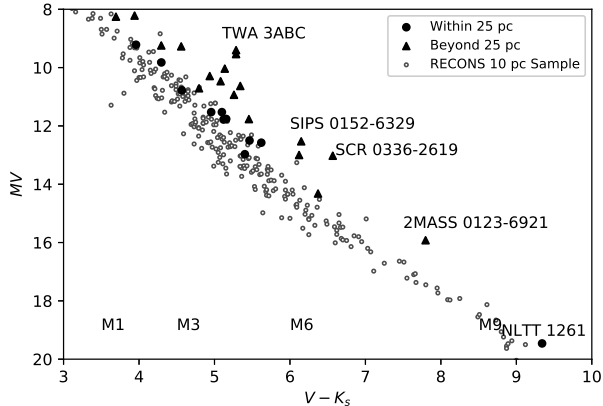


Figure 14. Color-Magnitude Diagram for the stars with follow-up astrometry and photometry from this paper, plotted against the RECONS 10 pc sample. A substantial number of stars lie beyond 25 pc of the Sun, and are more than a magnitude overluminous compared to the mostly main-sequence stars in the RECONS 10 pc sample.

M giants, which makes it an easy diagnostic to use in luminosity classifying.

The Na I index is particularly useful for determining the relative surface gravities of mid and cool M dwarfs (Schlieder et al. 2012). For our purposes, we use the Lyo et al. (2004) index constructed from a 24\AA wide region redward of the Na I 8200\AA doublet divided by a 24\AA wide region containing the Na I 8200\AA doublet, as used in Murphy et al. (2010), Riedel et al. (2011), Murphy et al. (2013), Rodriguez et al. (2013), and Riedel et al. (2014). Empirically, we have found that an index of 1.02 or less indicates a giant (see Figure 15), and intermediate index values between dwarfs (which increase to lower temperatures) and giants (which remain flat at 1.02) indicate a low-surface-gravity pre-main-sequence star. The results for this sample of stars are shown in Figure 15.

Unfortunately, giants and dwarfs overlap at colors bluer than $V - K_s = 5$. Alkali metal lines such as Na I can also be affected by stellar activity, where emission fills in the absorption line cores, leading to lower EWs (Reid & Hawley 1999). Slesnick et al. (2006) notes that the Na I doublet can be affected by telluric absorption over the region $8161\text{--}8282\text{\AA}$, leading to artificially low Na I index values for stars observed at large airmasses. Our results have large systematic errors because of this uncorrected telluric absorption.

We also use the K I 7699\AA doublet line (though not its companion at 7665\AA , because that portion of the spectrum is contaminated by the atmospheric A band) equivalent width as an independent indicator of surface gravity. As with the Na I index, the K I values for giants

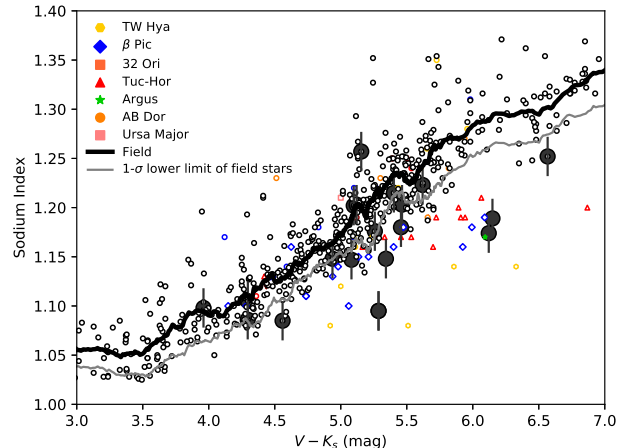


Figure 15. The Na I Index from Lyo et al. (2004) versus $V - K_s$. TINYMO objects measured spectroscopically are shown as large black points with error bars; the smaller points are young stars from Riedel et al. (2017b) and other RECONS spectral holdings measured with MATCHSTAR. A 25-point moving average (thick black line) and standard deviation (gray line) show the boundaries of inactive stars, and demonstrate that many of our targets have lower surface gravities than typical field stars, though many are consistent with or even higher than the field locus.

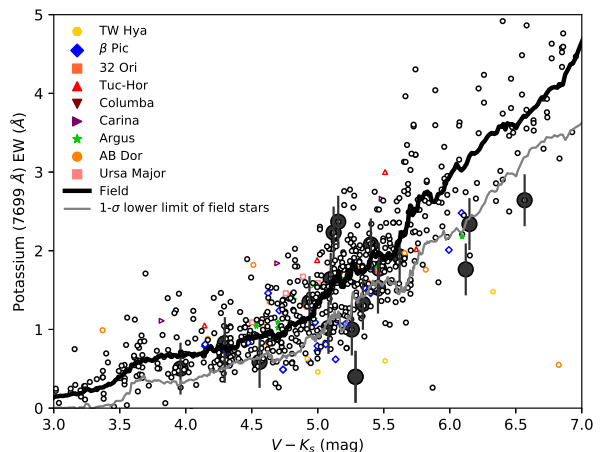


Figure 16. The same as Figure 15, except showing the K I equivalent width.

and dwarfs overlap at colors bluer than $V - K_s = 5$. Those results are shown in Figure 16.

Many of the stars in this sample have $H\alpha$ in emission (see Figure 17). As noted by West et al. (2008) and Zuckerman & Song (2004), $H\alpha$ activity persists in M dwarfs for long periods of time, which means $H\alpha$ itself is not a suitable source of youth. Strong $H\alpha$ emission

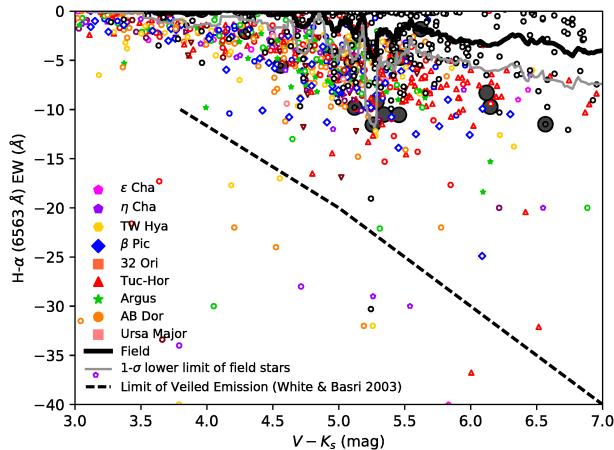


Figure 17. The same as Figure 15, except showing the H α EW, and the White & Basri (2003) limit (dotted black line) below which veiling from accretion is a probable concern.

has been linked to accretion and T Tauri status, but none of these stars comes close to the White & Basri (2003) limit.

The other available means for judging the youth of the stars studied here is kinematics, through which stars can be matched to nearby young moving groups (NYMGs) like β Pictoris (Song et al. 2002) and Tucana-Horologium (Zuckerman et al. 2001). CTIOPI astrometry provides accurate values of five of the six kinematic elements (RA, DEC, μ_{RA} , μ_{DEC} , and Parallax; missing only RV) necessary to fully describe a star’s position and motion. The LACEwING code (Riedel et al. 2017b) can accommodate partial information and calculate the probabilities of membership in 13 nearby young moving groups, and three nearby open clusters.

LACEwING has two modes of operation: Field and Young star mode. In Field star mode, the probabilities are calculated allowing for the possibility that the star is a field star with coincidentally similar space velocities to a young moving group (where field stars outnumber moving group members 50:1). In Young star mode, the probabilities are calculated assuming that the star is known to be spectroscopically or photometrically young, and young field stars are evenly matched with young moving group members, 1:1. We consider LACEwING membership probabilities of 20-50% to be low, 50-75% to be medium, and 75%-100% to be high probability memberships.

For objects with low surface gravity (below the gray lines in either Figure 15 or Figure 16), we have used LACEwING’s young star mode. For all other objects, we have used field star mode. We are accordingly bi-

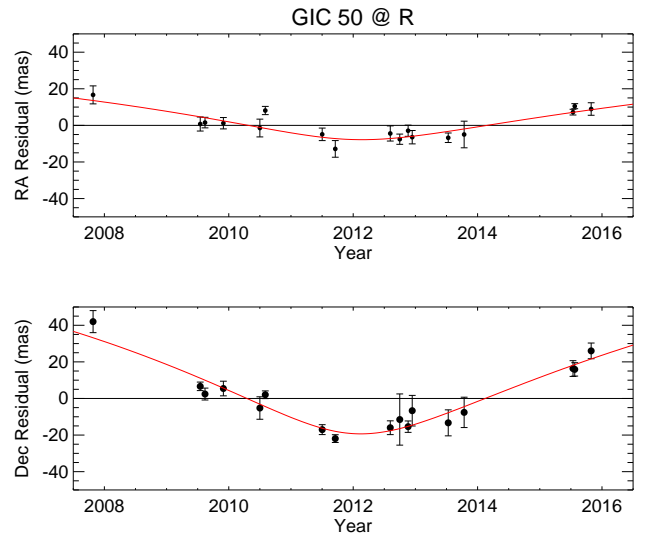


Figure 18. The perturbations in the astrometric residuals of GIC 50 (curve) due to its otherwise-unseen companion have been removed from the astrometry before the final parallax was fit.

ased against identifying members of AB Doradus (125 Myr) and older groups, where M dwarf surface gravities are indistinguishable from field stars. The results of this study, and spectroscopic measurements, are given in Table 7.6.

8. SYSTEM NOTES

Here we describe each of the 26 systems for which parallaxes are published in this paper in Table 4.4.1. See also Table 8 for details on the various multiple systems.

(0024-0158) *NLTT 1261*—BRI 0021-0214 ($M_V = 19.46$, $V - K_s = 9.34$) has $V = 19.88$, making it the faintest star in the optical *VRI* bandpasses in this survey. Our parallax (82.4 ± 2.2 mas) is consistent with that of Tinney et al. (1995) (86.6 ± 4.0 mas), and represents a factor of two improvement in the uncertainty.

(0032-0434) *GIC 50*—($M_V = 12.75$, $V - K_s = 5.62$) exhibits a perturbation due to an unseen companion spanning the full 8 years of our data, as shown in Figure 18. A fit has been made to the data and the perturbation removed to derive the astrometry results given in Table 4.4.1. The system was resolved with AstraLux by Janson et al. (2014), who found it to be a triple with companions at $0.508''$ and $0.213''$.

(0112+1703) *2MA 0112+1703*—($M_V = 10.71$, $V - K_s = 4.79$) was identified by Malo et al. (2013) as a potential member of AB Dor, but the identification was less certain because the star had no measured parallax or radial velocity. While Malo et al. (2014) furnished a ra-

Table 8. Multiple Star Results

Name	Binary Type	Separation	Position Angle	Δ Mag.	Filter	Ref.
(1)	(2)	(3)	(4)	(5)	(6)	(7)
GIC 50	AB	VB	0.51	184		<i>z'</i> Janson et al. (2014)
GIC 50	AB	VB	0.21	17		<i>z'</i> Janson et al. (2014)
2MASS 0123-6921						
2MASS 0254-5103	AB	VB	15.3	80.2	5.48	<i>V</i>
2MASS 0446-1116	AB	VB	~1.0	~285	~0.9	<i>V</i>
SCR 0533-4257	AB	IB	0.056	?	0.7	<i>F583W</i>
2MASS 0936-2610	AB	VB	41	314	3.25	<i>K</i>
2MASS 0936-2610	AC	VB	0.39	284	0.5	? (B. Mason, Priv. Comm.)
SIPS 1110-3731	AB	VB	~1.16	~209	~0.38	<i>V</i>
SIPS 1110-3731	AC	SB				Webb et al. (1999)
Stephenson 164						
GJ 2122	AB	VB	0.59	255	2	<i>V</i> Heintz (1987)
UPM 1710-5300	AB	VB	~0.77	~343	~0.69	<i>V</i>
DENIS 1956-3207	AB	VB	26.37	43.9	1.71	<i>V</i>

NOTE—Measurements are this work unless otherwise noted. AB= Astrometric Binary, IB= Interferometric Binary, SB = Spectroscopic Binary, VB = Visual Binary. Approximate measurements were determined by eye.

dial velocity, this is the first parallax. With all available information, the system is still a high probability member of AB Dor. We do not have a spectrum of 2MA 0112+1703, but AB Dor members are too old to distinguish from field stars by Na I or K I surface gravity, so a spectrum would not be expected to show any of the signs of youth we are looking for.

(0123-6921) 2MA 0123-6921—($M_V = 15.92, V - K_s = 7.80$) is a color-magnitude diagram match (we have no spectrum to measure its $H\alpha$ or gravity features) for the TW Hydra association, but like SCR 0103-5515 and SCR 0336-2610 in Riedel et al. (2014), this system is on the wrong side of the sky from all known members. It is kinematically consistent with Tuc-Hor and to a lesser extent AB Dor, but would have to be a higher-order multiple to align with other members of those groups on the HR diagram. We conclude that the system must be young and assign it to Tuc-Hor, and note that it is likely to be a triple or quadruple in that case, but find no evidence in our astrometric data.

(0128-1458) SCR 0128-1458—($M_V = 12.97, V - K_s = 5.40$) shows a possible perturbation in the 6 years of data available, but only in the DEC axis (Figure 19) More data are required before the companion can be confirmed. Regardless, a fit has been made to the data

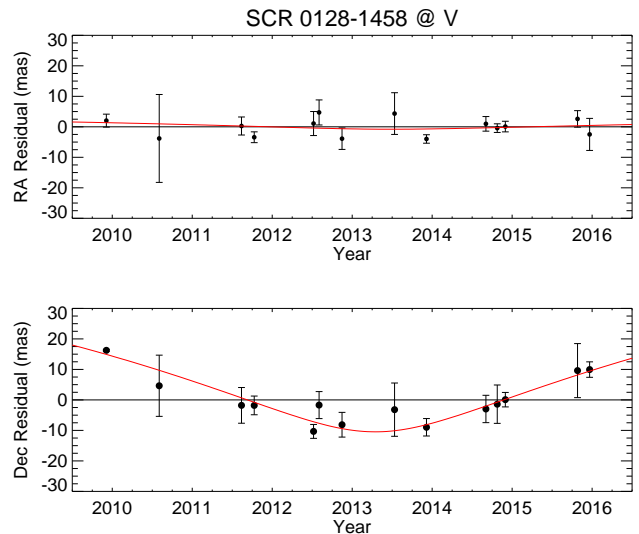


Figure 19. Same as Figure 18, but for the star SCR0128-1458. There is no visible perturbation on the RA axis.

and the slight possible perturbation removed to derive the astrometry results given in Table 4.4.1.

(0135-0712) BAR 161-012—($M_V = 10.63, V - K_s = 5.34$) flared to a maximum of 193 mmag in *R* on UT 11 Oct 2011, and shows a variability of 51 mmag over the 5 year dataset, as shown in Figure 20. This photometric

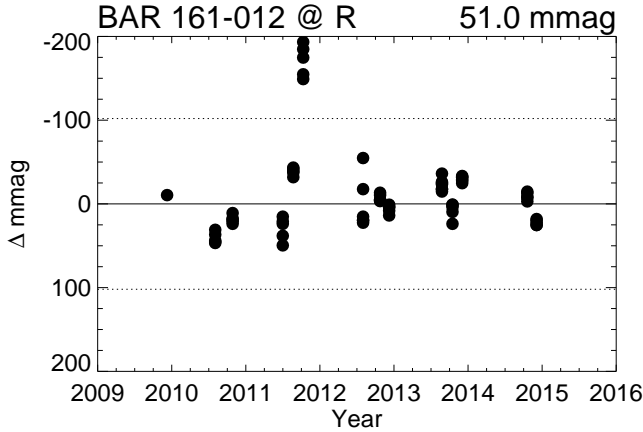


Figure 20. Relative R -band photometry of BAR 161-012 from 2009-2015. A flare can be seen on 11 Oct 2011, as well as generally high photometric variability (>20 mmag).

variability and a discrepancy between a photometric distance estimate of 12.3 pc and a trigonometric distance of 36.1 pc indicates that this star is likely young. While several sources, most notably [Shkolnik et al. \(2012\)](#), place this star in β Pic, we find that this star’s kinematics are inconsistent with any known NYMG. This star is yet another young star without membership in a NYMG.

(0143-0602) SCR 0143-0602—($M_V = 11.53, V - K_s = 5.10$) was observed to be 178 mmag in V above its baseline brightness on UT 18 Oct 2014, although the peak may have been higher because this offset was measured in the first frame taken that night. The star’s photometric variability is 37 mmag over 5 years, indicating it might be young. The discrepancy between the photometric distance estimate of 13.3 pc and trigonometric distance of 19.8 pc also hints that the star might be young, or alternately, an unresolved multiple.

(0152-6329) SIP 0152-6329—($M_V = 12.53, V - K_s = 6.15$) is a new Tuc-Hor member as identified by kinematics and the sodium gravity test, with a LACEwING-derived membership probability of 80%. [Gagné et al. \(2015\)](#) found it to be a member of β Pic, but we find only an 11% probability of this. We do not find the star to be significantly photometrically variable in R over 7 years.

(0222-6022) SCR 0222-6022—($M_V = 10.93, V - K_s = 5.26$) was first identified as a member of Tuc-Hor by [Rodríguez et al. \(2013\)](#). It is confirmed as a member based on kinematics (with 88% probability in LACEwING) and both gravity tests. The star varies by 41 mmag over 5 years, as shown in Figure 22, supporting the premise that it is young.

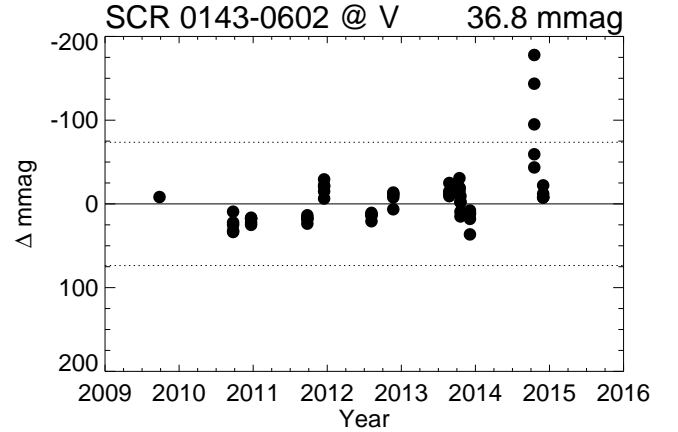


Figure 21. Same as Figure 20, but for SCR 0143-0602. A flare can be seen on UT 17 Oct 2014.

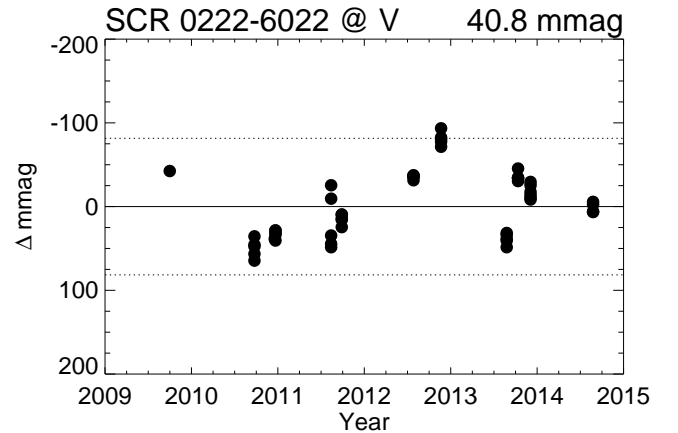


Figure 22. Same as Figure 20, but for SCR 0222-6022.

(0236-5203) 2MA 0236-5203—($M_V = 9.27, V - K_s = 4.56$) has a proper motion of 80 mas/yr at position angle 97° , similar to the 2MA 0254-5108AB system (discussed next) with 87 mas yr^{-1} at 93° . 2MA 0236-5203 was identified in [Zuckerman & Song \(2004\)](#) as a Tuc-Hor member, and we find it to be a member of that group via kinematics.

This star does show a photometric variability of 40 mmag as shown in Figure 23, indicative of youth, which corroborates the low surface gravity measurement from the sodium index.

(0254-5108) 2MA 0254-5108AB—($M_V = 9.24, V - K_s = 4.29(A), M_V = 14.32, V - K_s = 6.37(B)$) is a binary with a separation of $15.3''$ at a position angle of 80.2° . We do not see any indication of orbital motion of the components in the 5 year timespan of our observations. The two components have the largest ΔV (5.48) of any resolved system under consideration here; the astrom-

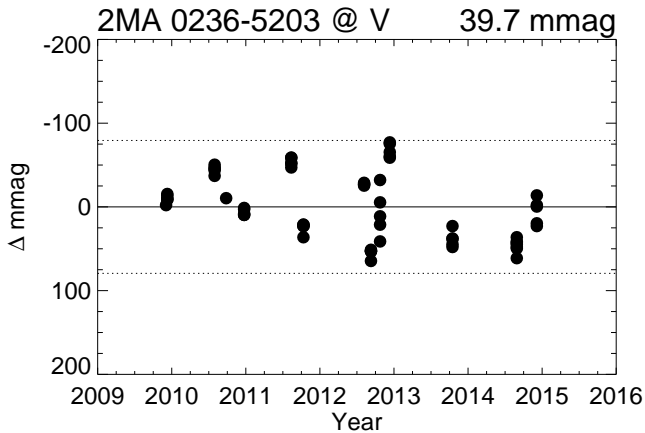


Figure 23. Same as Figure 20, but for 2MA 0236-5203.

etry for the B component suffers due to its low SNR because images were taken based on the brightness of the A component. The trigonometric parallaxes differ by 1.9σ , which may be caused by the low signal on B, or (alternately) taken as evidence that these are two separate members of Tuc-Hor serendipitously aligned on the sky. Assuming they are a bound system (and with the weighted mean system parallax), the A component is only marginally consistent with Tuc-Hor membership and would need to be an equal-luminosity binary to fit the Tuc-Hor isochrone. Currently, the agreement with Tuc-Hor (for both components) actually improves if the parallaxes are *not* combined, and the two components are treated as separate star systems. The single ROSAT X-ray detection is likely for the A component.

Both of the stars are variable, by 51 mmag (A) and 46 mmag (B) in V over 5 years, although the variability for B is suspect given its low level of counts throughout the observing sequence. Component A flared to a maximum of 255 mmag above its mean value on UT 31 Jul 2012 (Figure 24). Both stars are almost certainly young, supported by the parallaxes that place them well above the main sequence — photometric estimates place the stars at 21 pc (A) and 31 pc (B), whereas the trigonometric distances are 37 pc and 45 pc, respectively.

(0336-2619) *SCR 0336-2619*—($M_V = 13.02, V - K_s = 6.57$) is a member of Tuc-Hor, as first suggested by Gagné et al. (2015). Despite its clear spectroscopic signatures of gravity and chromospheric activity, it has an exceptionally flat lightcurve, shown in Figure 25.

(0413-0139) *RX 0413-0139*—($M_V = 11.77, V - K_s = 5.46$) exhibits photometric variability at the 35 mmag level over 5 years, as shown in Figure 26. The astrometric residuals are poor (~ 9.5 mas) in the DEC axis due to few reference stars in the southern portion of the field.

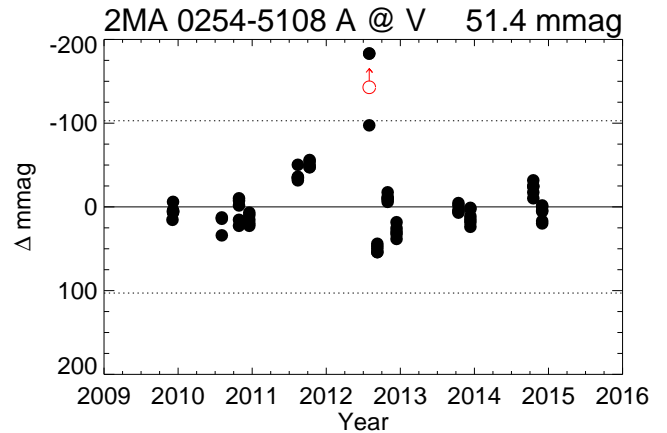


Figure 24. Same as Figure 20 but for 2MA 0254-5108A. A flare is seen on 31 Jul 2012. One photometric point (indicated in red) from that sequence is outside the scale of the figure.

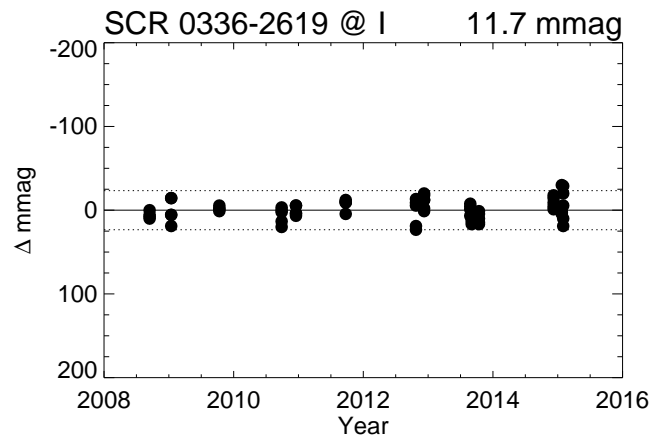


Figure 25. Same as Figure 20 but for SCR 0336-2619.

RX 0413-0139 was reported to be a member of the Argus association by Malo et al. (2013), but we find no support for that identification using our new parallax. This star and BAR 161-012 are new examples of nearby young stars without membership in any known group.

(0446-1116) *2MA 0446-1116AB*—($M_V = 11.53, V - K_s = 4.96$) appears elongated in our images, with two components separated by $\sim 1''.0$. This companion is too close to be properly centroided or even distinguished from the primary, which results in a parallax with a relatively high error of 3.4 mas that is unlikely to improve with additional data from our observing program.

(0510-7236) *HD 271076*—($M_V = 9.82, V - K_s = 4.30$) was reasonably suspected to be a supergiant in the LMC by Westerlund et al. (1981) given its location in the sky. However, at a distance of 20.2 ± 1.1 pc it is clearly a fore-

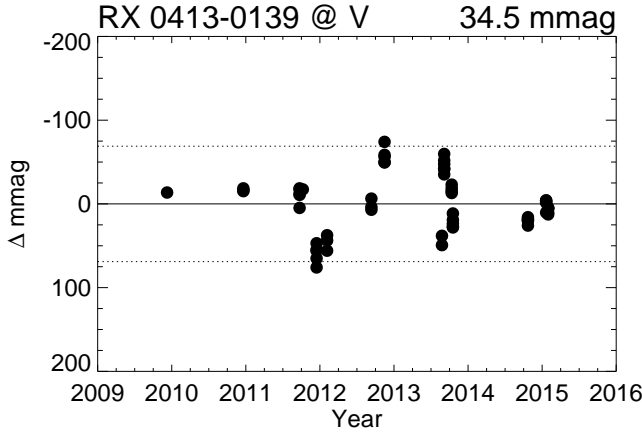


Figure 26. Same as Figure 20 but for RX 0413-0139.

ground M2.0V star and a member of the Solar Neighborhood. Much of the error in the parallax (2.8 mas) can be attributed to a faint reference field.

(0533-4257) SCR 0533-4257AB—($M_V = 12.50$, $V - K_s = 5.46$) is the closest system in our sample, at a distance of only 10.4 ± 0.1 pc. It has a very low proper motion, only 39 mas yr^{-1} . The relatively large position angle error (1.5 deg) in Table 4.4.1 is due to this small proper motion; the proper motion errors themselves are no worse than for other stars on the program.

The system was identified in Riaz et al. (2006) to emit X-rays, so we observed it during our HST-FGS Cycle 16B campaign. It was resolved (Figure 27) into a close binary with a 56 mas separation and $\Delta F583W = 0.7$ mag on 2 Dec 2008. Thus, the stars have a projected separation of roughly 0.56 AU, and the system’s X-ray flux is unlikely to be due to the components’ interactions. A periodogram of our astrometric data shows a peak with a period near 9 months, consistent with the projected separation for the companion in a Keplerian orbit. However, the amplitude of the perturbation is small and evident in the RA direction only, so we present an uncorrected parallax in Table 4.4.1.

Given the system’s X-ray emission, it is probably at least somewhat youthful, but based on its lack of low-gravity features and color-magnitude diagram position (corrected for its multiplicity), the system is over 120 Myr old. The kinematics of the system do not place it in any of the nearby young moving groups.

(0639-2101) LP 780-32—($M_V = 11.78$, $V - K_s = 5.12$) has a photometric distance estimate of 11.6 pc, which places the system closer than the parallax (15.8 pc). Kinematic analysis shows it to be a low-probability member of Argus.

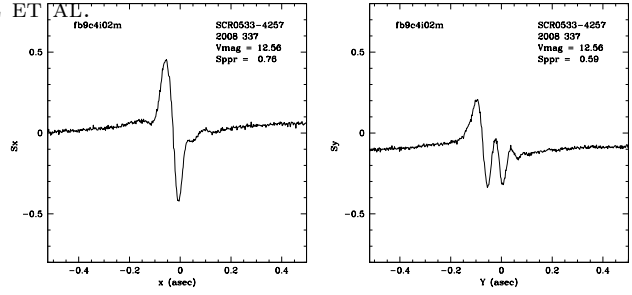


Figure 27. The X-axis (left) and Y-axis (right) Hubble Space Telescope Fine Guidance Sensor preliminary results for SCR 0533-4257AB. The Y-axis “S-curve” of the Fine Guidance Sensor shows a second dip to the right of the main one, revealing a companion. The companion can also be identified as a deformation in the in the X-axis S curve, compared to a single star, though it is not visibly apparent. Figure by Ed Nelan.

(0936-2610) 2MA 0936-2610ABC—($M_V = 11.76$, $V - K = 5.15$, $M_K = 6.61(A)$, $M_K = 9.86(B)$) is a likely common proper motion binary separated by $41''$ at position angle 314° . While comparing images from multiple epochs (SuperCOSMOS, 2MASS, and WISE images) using Aladin, we discovered the possible secondary, which is not in SIMBAD. We are unable to determine a reliable proper motion or parallax for the companion using our existing data because it is 3.2 mag fainter than the primary at K , and not exposed well enough in our images at V for reliable astrometry. With $VRI = 13.11$, 11.86, 10.31 and $JHK = 8.86$, 8.29, 7.96, we estimate a photometric distance of 17.0 ± 2.7 pc for the possible companion, which is consistent with the trigonometric distance of 18.6 pc for A. The A component’s photometric distance is closer, 13.6 ± 2.2 pc. Speckle observations from 2010 (B. Mason, private communication) indicate the A component may be a close binary at $0'39$ at 284 degrees with a delta mag of 0.5. No sources were near the star at either the Palomar Deep Sky Survey (DSS) 1 red plate epoch (1955) or DSS2 red plate epoch (1995), making it likely that the speckle source is a co-moving companion and the system as a whole is a triple.

(1110-3731) SIP 1110-3731ABC=TWA 3ABC—($M_V = 9.40$, $V - K_s = 5.29$), is one of the first known members of the TW Hya association (de la Reza et al. 1989), and has for some time been considered the closest genuine member (TWA 22AB, at 17.5 ± 0.2 pc, is now widely believed to be a member of β Pic instead, Mamajek 2005; Teixeira et al. 2009.) Webb et al. (1999) and Zuckerman & Song (2004) claim that this system is a triple (see Table 8) where A is a spectroscopic binary, presumably SB2; with no other information given we assume $\Delta V = \Delta K = 0$, which makes B the actual brightest component.

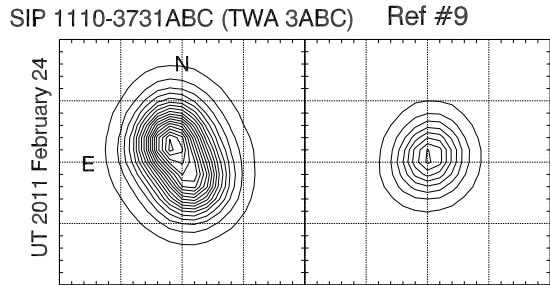


Figure 28. Positions of TWA 3 AC (NE) and B (SW) on 24 Feb 2011. As seen here, TWA 3B often appears as a mere elongation of the TWA 3AC PSF, making parallax reduction difficult. Reference star #9 is shown on the right as an example single-star PSF, with the same contour intervals. Grid lines are $2.05''$ apart, or 5 pixels at the CTIO 0.9m.

As shown in Figure 28, we detect two nearly equal magnitude sources separated by $1''.16$ at a position angle of 210.2° , which implies a projected separation of 38 AU. During reductions, many frames were thrown out and most of the remaining SExtractor output had to be manually edited to correctly identify the B component. The resulting parallax precision for the two components in Table 4.4.1 is poor, with errors of 4.0 and 6.8 mas, and the measured variability is unreliable. Nevertheless, the combined weighted mean result of 33 pc is close to the expected distance to the system (42 pc) based on kinematics in Zuckerman & Song (2004). The astrometry also confirms that each star is a potential member of the TW Hydra association, though only TWA 3B has a published radial velocity consistent with the predicted best-fit value.

We see minimal evidence for orbital motion in the form of different proper motions for the two components. We find the difference to be marginally significant: $\Delta\mu_{RA \cos DEC} = 20 \pm 11 \text{ mas yr}^{-1}$, $\Delta\mu_{DEC} = 35 \pm 12 \text{ mas yr}^{-1}$. The separation of the two components in our images on 02 Apr 2012 is $1.16''$ at position angle 210.2° , but aperture photometry for each component is not possible with our data. Instead, a PSF fit of the photometry data for each component is used to apply the DCR correction that is the same for both components, consistent with their similar $V - I$ colors.

(1206-1314) STEPH 164—($M_V = 10.29$, $V - K_s = 4.94$) exhibits a possible perturbation in the somewhat limited set of data we have spanning 4 years. The discrepancy between photometric (14.2 pc) and trigonometric distance (31.0 pc) also implies the object might be a young star and/or an unresolved multiple star. As neither kinematics nor spectroscopy identify it as a young object, we suspect this star is a multiple star system.

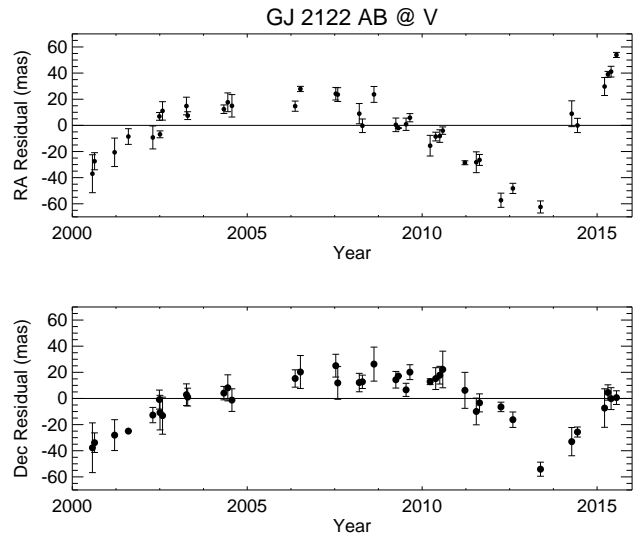


Figure 29. Same as Figure 18, but for the star GJ2122AB. Large astrometric perturbations are seen in both axes.

(1645-3848) GJ 2122AB—($M_V = 9.29$, $V - K_s = 3.96$) was found by Heintz (1987) to be a binary with separation $0.59''$ and an estimated by-eye delta magnitude of 2.0. (see Table 8) We see a single source in our images spanning 16 years, but find it to be an obvious astrometric binary, as shown in the nightly mean residuals of the positions after the parallax and proper motion fit (Figure 29). Although the orbital period remains uncertain, the parallax given in Table 4.4.1 has been derived after removing our best approximation to the perturbation measured to date. Our calculated correction to absolute is an unrealistic $5.08 \pm 1.34 \text{ mas}$ because of a reddened reference field, so we have adopted a generic correction of $1.5 \pm 0.5 \text{ mas}$, and find the system to be at a distance of 12.4 pc.

The binary is also known as HIP 82021, but a bad position (off by $19''$, more than the scale of the astrometer grating) in the Hipparcos Input Catalog (Turon et al. 1993) leads to an enormous parallax error, and it was omitted from both official HIPPARCOS catalogs. Fabricius & Makarov (2000) re-reduced the HIPPARCOS data and found a parallax of poor quality ($71.3 \pm 14.8 \text{ mas}$, $14.0 \pm 2.9 \text{ pc}$) and again blame the pointing error. Our parallax result ($77.2 \pm 2.1 \text{ mas}$, $13.0 \pm 0.3 \text{ pc}$) is consistent with the Fabricius & Makarov (2000) result. (There is as yet no result from Gaia for this star, likely for the same reason.)

(1710-5300) UPM 1710-5300AB—($M_V = 10.78$, $V - K_s = 4.57$) is a binary for which we estimate a separation of $0''.8$ (see Table 8). The system appears as one elongated source in our data, and we determine a single

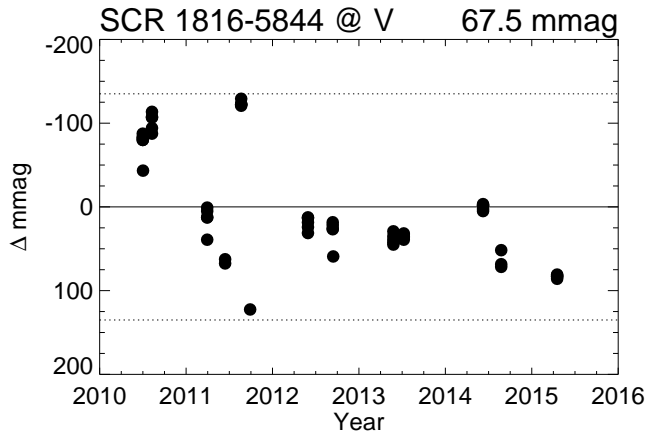


Figure 30. Same as Figure 20 but for SCR1816-5844.

parallax for the combined system with relatively high error (3.0 mas).

(1809-7613) *SIPS 1809-7613*—($M_V = 13.00$, $V - K_s = 6.12$) is a possible member of β Pictoris, as determined by a low-probability LACEwing membership of 31%, supported by low-gravity features in both sodium and potassium. The photometric variability is measured to be very low at 9 mmag, but frames were taken in the I filter, where variability is lower than in V or R .

(1816-5844) *SCR 1816-5844*—($M_V = 10.47$, $V - K_s = 5.08$) is a new member of Argus, according to kinematics, corroborated by the sodium and potassium line strengths indicative of low surface gravity. This star exhibits the highest level of photometric variability of any star reported here — 68 mmag at V over the 5 years, as shown in Figure 30. This youth indicator is supported by the discrepancy between a photometric distance of 12.2 pc and a trigonometric distance of 29.0 pc, placing the star well above the main sequence in the HR diagram.

(1956-3207) *DEN 1956-3207AB*—($M_V = 8.254$, $V - K_s = 3.69(A)$, $M_V = 10.04$, $V - K_s = 5.14(B)$) is a binary separated by $26''$ for which we determine separate but entirely consistent parallaxes placing the system at 45 pc. We do not have spectroscopy of either member of this system with which to comment on its age, but kinematic analysis with LACEwing shows no probability of membership in any known NYMG. The A component shows significant photometric variability of 31 mmag at V , while B’s variability of 20 mmag is more muted. This system does not seem to be young.

(2332-1215) *BD-13 06424*—($M_V = 8.22$, $V - K_s = 3.94$) is a known member of β Pic (Torres et al. 2006), which we confirm with our astrometric results (Table 4.4.1).

We find the star to be photometrically variable at V at a level of 28 mmag during the 5 years of data in hand.

9. CONCLUSIONS

The effort described in this paper was an experiment to determine whether or not we might reveal nearby stars via a completely photometric search, rather than via the traditional route of assuming high proper motions. The combination of optical photometry from SuperCOSMOS and infrared photometry from 2MASS proved to be a powerful method to find nearby stars with minimal proper motions. In this paper, we report:

- 29 parallaxes for 26 stellar systems, including 11 systems within 25 pc and 15 between 25 and 50 pc. The closest three systems are between 10 and 12.5 pc distant. All of the systems have $\mu = 38$ –179 mas yr $^{-1}$, which is slower moving than the 180 mas yr $^{-1}$ threshold used by Luyten for his compendia of proper motion stars. Thus, the experiment to find nearby, slow-moving stars, was successful.

- 12 pre-main sequence stellar systems that are identified to be part of the AB Doradus (two systems), Argus (three system), Tucana-Horologium (5), β Pictoris (1), and TW Hydra (1) moving groups, plus two additional stars that do not appear to be associated with any group. The unassociated stars (along with other young non-members identified in Riedel et al. 2014 and Riedel et al. 2017a) hint at a complex outcome to the star formation process that yields relatively young stars that cannot be straightforwardly linked to known associations or moving groups.

- Among those stars is LP 780-032, another possible new member of the Argus moving group at a distance of only 15 pc. This system would rank as the fifth closest young star system.

The RECONS effort has been supported by the National Science Foundation through grants AST 05-07711, AST 09-08402, and AST 14-12026. We also thank the members of the SMARTS Consortium and the CTIO staff, who enable the operations of the small telescopes at CTIO. This research has made use of results from the SAO/NASA Astrophysics Data System Bibliographic Services, as well as the SIMBAD and VizieR databases operated at CDS, Strasbourg, France, and the Two Micron All Sky Survey, which is a joint project of the University of Massachusetts and the Infrared Processing and Analysis Center, funded by NASA and NSF. The authors would like to thank the HST and Lowell Observatory staff, and Ed Nelan, for their assistance with data collection and processing.

Facility: CTIO:0.9m, CTIO:1.5m (RCSpec), Blanco (RCSpec), Perkins (DeVeny Spectrograph), CFHT (ES-PaDONs), HST (FGS)

Software: Astropy (Astropy Collaboration et al. 2013), Numpy (Walt et al. 2011), Matplotlib (Hunter 2007), IRAF, MATCHSTAR (Riedel et al. 2014), LACEwING (Riedel et al. 2017b)

REFERENCES

- Alksnis, A., Balklavs, A., Dzervitis, U., et al. 2001, *Baltic Astronomy*, 10, 1
- Allers, K. N., Jaffe, D. T., Luhman, K. L., et al. 2007, *ApJ*, 657, 511, doi: [10.1086/510845](https://doi.org/10.1086/510845)
- Astropy Collaboration, Robitaille, T. P., Tollerud, E. J., et al. 2013, *A&A*, 558, A33, doi: [10.1051/0004-6361/201322068](https://doi.org/10.1051/0004-6361/201322068)
- Aumer, M., & Binney, J. J. 2009, *MNRAS*, 397, 1286, doi: [10.1111/j.1365-2966.2009.15053.x](https://doi.org/10.1111/j.1365-2966.2009.15053.x)
- Backman, D. E., Burgh, S. J., & Henry, T. J., eds. 2001, *Nearby Stars (NStars) Workshop*
- Bessel, F. W. 1838, *MNRAS*, 4, 152
- Bessell, M. S. 1986, *PASP*, 98, 1303, doi: [10.1086/131934](https://doi.org/10.1086/131934)
- Bobylev, V. V. 2010, *Astronomy Letters*, 36, 220, doi: [10.1134/S1063773710030060](https://doi.org/10.1134/S1063773710030060)
- Boeshaar, P. C. 1976, *The spectral classification of m-dwarf stars* (Columbus: Ohio State University, 1976)
- Boyd, M. R., Henry, T. J., Jao, W.-C., Subasavage, J. P., & Hambly, N. C. 2011a, *AJ*, 142, 92, doi: [10.1088/0004-6256/142/3/92](https://doi.org/10.1088/0004-6256/142/3/92)
- Boyd, M. R., Winters, J. G., Henry, T. J., et al. 2011b, *AJ*, 142, 10, doi: [10.1088/0004-6256/142/1/10](https://doi.org/10.1088/0004-6256/142/1/10)
- Cruz, K. L., Reid, I. N., Kirkpatrick, J. D., et al. 2007, *AJ*, 133, 439, doi: [10.1086/510132](https://doi.org/10.1086/510132)
- Cutri, R. M., Skrutskie, M. F., van Dyk, S., et al. 2003, *2MASS All Sky Catalog of point sources*. (NASA/IPAC Infrared Science Archive. <http://irsa.ipac.caltech.edu/applications/Gator/>)
- de la Reza, R., Torres, C. A. O., Quast, G., Castilho, B. V., & Vieira, G. L. 1989, *ApJ*, 343, L61, doi: [10.1086/185511](https://doi.org/10.1086/185511)
- Deacon, N. R., & Hambly, N. C. 2007, *A&A*, 468, 163, doi: [10.1051/0004-6361:20066844](https://doi.org/10.1051/0004-6361:20066844)
- Deacon, N. R., Hambly, N. C., & Cooke, J. A. 2005, *A&A*, 435, 363, doi: [10.1051/0004-6361:20042002](https://doi.org/10.1051/0004-6361:20042002)
- Deacon, N. R., Hambly, N. C., King, R. R., & McCaughrean, M. J. 2009, *MNRAS*, 394, 857, doi: [10.1111/j.1365-2966.2008.14371.x](https://doi.org/10.1111/j.1365-2966.2008.14371.x)
- Dyson, Sir, F. W. 1917, *MNRAS*, 77, 212
- Fabricius, C., & Makarov, V. V. 2000, *A&AS*, 144, 45, doi: [10.1051/aas:2000198](https://doi.org/10.1051/aas:2000198)
- Finch, C. T., Henry, T. J., Subasavage, J. P., Jao, W., & Hambly, N. C. 2007, *AJ*, 133, 2898, doi: [10.1086/518164](https://doi.org/10.1086/518164)
- Fitzpatrick, E. L. 1999, *PASP*, 111, 63, doi: [10.1086/316293](https://doi.org/10.1086/316293)
- Gagné, J., Lafrenière, D., Doyon, R., Malo, L., & Artigau, É. 2015, *ApJ*, 798, 73, doi: [10.1088/0004-637X/798/2/73](https://doi.org/10.1088/0004-637X/798/2/73)
- Gaia Collaboration, Brown, A. G. A., Vallenari, A., et al. 2016, *A&A*, 595, A2, doi: [10.1051/0004-6361/201629512](https://doi.org/10.1051/0004-6361/201629512)
- Giclas, H. L., Burnham, Jr., R., & Thomas, N. G. 1979, *Lowell Observatory Bulletin*, 8, 145
- Gizis, J. E. 1997, *AJ*, 113, 806, doi: [10.1086/118302](https://doi.org/10.1086/118302)
- Gliese, W., & Jahreiß, H. 1991, *Preliminary Version of the Third Catalogue of Nearby Stars*, Tech. rep.
- Hambly, N. C., Davenhall, A. C., Irwin, M. J., & MacGillivray, H. T. 2001a, *MNRAS*, 326, 1315, doi: [10.1046/j.1365-8711.2001.04662.x](https://doi.org/10.1046/j.1365-8711.2001.04662.x)
- Hambly, N. C., Henry, T. J., Subasavage, J. P., Brown, M. A., & Jao, W. 2004, *AJ*, 128, 437, doi: [10.1086/421748](https://doi.org/10.1086/421748)
- Hambly, N. C., MacGillivray, H. T., Read, M. A., et al. 2001b, *MNRAS*, 326, 1279, doi: [10.1046/j.1365-8711.2001.04660.x](https://doi.org/10.1046/j.1365-8711.2001.04660.x)
- Heintz, W. D. 1987, *ApJS*, 65, 161, doi: [10.1086/191221](https://doi.org/10.1086/191221)
- Henderson, T. 1839, *MNRAS*, 4, 168
- Henry, T. J., Jao, W., Subasavage, J. P., et al. 2006, *AJ*, 132, 2360, doi: [10.1086/508233](https://doi.org/10.1086/508233)
- Henry, T. J., Kirkpatrick, J. D., & Simons, D. A. 1994, *AJ*, 108, 1437, doi: [10.1086/117167](https://doi.org/10.1086/117167)
- Henry, T. J., Subasavage, J. P., Brown, M. A., et al. 2004, *AJ*, 128, 2460, doi: [10.1086/425052](https://doi.org/10.1086/425052)
- Henry, T. J., Walkowicz, L. M., Barto, T. C., & Golimowski, D. A. 2002, *AJ*, 123, 2002, doi: [10.1086/339315](https://doi.org/10.1086/339315)
- Høg, E., Fabricius, C., Makarov, V. V., et al. 2000, *A&A*, 355, L27
- Hunter, J. D. 2007, *Computing in Science & Engineering*, 9, 90, doi: <http://dx.doi.org/10.1109/MCSE.2007.55>
- Janson, M., Bergfors, C., Brandner, W., et al. 2014, *The Astrophysical Journal Supplement Series*, 214, doi: [10.1088/0067-0049/214/2/17](https://doi.org/10.1088/0067-0049/214/2/17)
- Jao, W., Henry, T. J., Subasavage, J. P., et al. 2005, *AJ*, 129, 1954, doi: [10.1086/428489](https://doi.org/10.1086/428489)
- Jao, W.-C., Henry, T. J., Subasavage, J. P., et al. 2003, *AJ*, 125, 332, doi: [10.1086/345515](https://doi.org/10.1086/345515)
- Keenan, P. C., & McNeil, R. C. 1976, *An atlas of spectra of the cooler stars: Types G,K,M,S, and C. Part 1: Introduction and tables* (Columbus: Ohio State University Press, 1976)

- Kirkpatrick, J. D., Henry, T. J., & McCarthy, Jr., D. W. 1991, *ApJS*, 77, 417, doi: [10.1086/191611](https://doi.org/10.1086/191611)
- Landolt, A. U. 1992, *AJ*, 104, 340, doi: [10.1086/116242](https://doi.org/10.1086/116242)
- . 2007, *AJ*, 133, 2502, doi: [10.1086/518000](https://doi.org/10.1086/518000)
- Leggett, S. K., Allard, F., Geballe, T. R., Hauschildt, P. H., & Schweitzer, A. 2001, *ApJ*, 548, 908, doi: [10.1086/319020](https://doi.org/10.1086/319020)
- Lepine, S., & Gaidos, E. 2013, in *American Astronomical Society Meeting Abstracts*, Vol. 221, American Astronomical Society Meeting Abstracts #221, 423.01
- Lépine, S., Rich, R. M., & Shara, M. M. 2005, *ApJ*, 633, L121, doi: [10.1086/498504](https://doi.org/10.1086/498504)
- Lépine, S., & Shara, M. M. 2005, *AJ*, 129, 1483, doi: [10.1086/427854](https://doi.org/10.1086/427854)
- Luyten, W. J. 1957, *A catalogue of 9867 stars in the Southern Hemisphere with proper motions exceeding 0."2 annually.* (Minneapolis, Lund Press, 1957.)
- . 1979, *NLTT catalogue. Volume.I. +90_to_+30_*. Volume.II. +30_to_0_ (Publ. by Univ. Minnesota, Minneapolis, USA. Vol. I: 282 p., Vol. II: 286 p.)
- Lyo, A.-R., Lawson, W. A., & Bessell, M. S. 2004, *MNRAS*, 355, 363
- Malo, L., Artigau, É., Doyon, R., et al. 2014, *ApJ*, 788, 81, doi: [10.1088/0004-637X/788/1/81](https://doi.org/10.1088/0004-637X/788/1/81)
- Malo, L., Doyon, R., Lafrenière, D., et al. 2013, *ApJ*, 762, 88, doi: [10.1088/0004-637X/762/2/88](https://doi.org/10.1088/0004-637X/762/2/88)
- Mamajek, E. E. 2005, *ApJ*, 634, 1385, doi: [10.1086/468181](https://doi.org/10.1086/468181)
- Mihalas, D., & Binney, J. 1981, *Galactic astronomy: Structure and kinematics /2nd edition/* (San Francisco, CA, W. H. Freeman and Co., 1981. 608 p.)
- Murphy, S. J., Lawson, W. A., & Bessell, M. S. 2010, *MNRAS*, 406, L50. <https://arxiv.org/abs/1005.3308>
- . 2013, *MNRAS*, 435, 1325, doi: [10.1093/mnras/stt1375](https://doi.org/10.1093/mnras/stt1375)
- Nordström, B., Mayor, M., Andersen, J., et al. 2004, *A&A*, 418, 989, doi: [10.1051/0004-6361:20035959](https://doi.org/10.1051/0004-6361:20035959)
- Pokorny, R. S., Jones, H. R. A., & Hambly, N. C. 2003, *A&A*, 397, 575, doi: [10.1051/0004-6361:20021385](https://doi.org/10.1051/0004-6361:20021385)
- Reid, I. N., Cruz, K. L., & Allen, P. R. 2007, *AJ*, 133, 2825, doi: [10.1086/517914](https://doi.org/10.1086/517914)
- Reid, I. N., & Hawley, S. L. 1999, *AJ*, 117, 343
- Riaz, B., Gizis, J. E., & Harvin, J. 2006, *AJ*, 132, 866, doi: [10.1086/505632](https://doi.org/10.1086/505632)
- Riedel, A. R. 2012, PhD thesis, Georgia State University
- Riedel, A. R., Alam, M. K., Rice, E. L., Cruz, K. L., & Henry, T. J. 2017a, *ApJ*, 840, 87, doi: [10.3847/1538-4357/840/2/87](https://doi.org/10.3847/1538-4357/840/2/87)
- Riedel, A. R., Blunt, S. C., Lambrides, E. L., et al. 2017b, *AJ*, 153, 95, doi: [10.3847/1538-3881/153/3/95](https://doi.org/10.3847/1538-3881/153/3/95)
- Riedel, A. R., Murphy, S. J., Henry, T. J., et al. 2011, *AJ*, 142, 104, doi: [10.1088/0004-6256/142/4/104](https://doi.org/10.1088/0004-6256/142/4/104)
- Riedel, A. R., Finch, C. T., Henry, T. J., et al. 2014, *AJ*, 147, 85, doi: [10.1088/0004-6256/147/4/85](https://doi.org/10.1088/0004-6256/147/4/85)
- Rodriguez, D. R., Zuckerman, B., Kastner, J. H., et al. 2013, *ApJ*, 774, 101, doi: [10.1088/0004-637X/774/2/101](https://doi.org/10.1088/0004-637X/774/2/101)
- Röser, S., Schilbach, E., Piskunov, A. E., Kharchenko, N. V., & Scholz, R.-D. 2011, *A&A*, 531, A92+, doi: [10.1051/0004-6361/201116948](https://doi.org/10.1051/0004-6361/201116948)
- Samus, N. N., Durlevich, O. V., & et al. 2012, *VizieR Online Data Catalog*, 1, 2025
- Schlieder, J. E., Lépine, S., Rice, E., et al. 2012, *AJ*, 143, 114, doi: [10.1088/0004-6256/143/5/114](https://doi.org/10.1088/0004-6256/143/5/114)
- Schmidt, S. J., Cruz, K. L., Bongiorno, B. J., Liebert, J., & Reid, I. N. 2007, *AJ*, 133, 2258, doi: [10.1086/512158](https://doi.org/10.1086/512158)
- Scholz, R.-D., & Meusinger, H. 2002, *MNRAS*, 336, L49, doi: [10.1046/j.1365-8711.2002.05998.x](https://doi.org/10.1046/j.1365-8711.2002.05998.x)
- Schönrich, R., Binney, J., & Dehnen, W. 2010, *MNRAS*, 403, 1829, doi: [10.1111/j.1365-2966.2010.16253.x](https://doi.org/10.1111/j.1365-2966.2010.16253.x)
- Shkolnik, E., Liu, M. C., & Reid, I. N. 2009, *ApJ*, 699, 649, doi: [10.1088/0004-637X/699/1/649](https://doi.org/10.1088/0004-637X/699/1/649)
- Shkolnik, E. L., Anglada-Escudé, G., Liu, M. C., et al. 2012, *ApJ*, 758, 56, doi: [10.1088/0004-637X/758/1/56](https://doi.org/10.1088/0004-637X/758/1/56)
- Skuljan, J., Hearnshaw, J. B., & Cottrell, P. L. 1999, *MNRAS*, 308, 731, doi: [10.1046/j.1365-8711.1999.02736.x](https://doi.org/10.1046/j.1365-8711.1999.02736.x)
- Slesnick, C. L., Carpenter, J. M., Hillenbrand, L. A., & Mamajek, E. E. 2006, *AJ*, 132, 2665
- Song, I., Bessell, M. S., & Zuckerman, B. 2002, *ApJ*, 581, L43
- Subasavage, J. P., Henry, T. J., Bergeron, P., et al. 2007, *AJ*, 134, 252, doi: [10.1086/518739](https://doi.org/10.1086/518739)
- Subasavage, J. P., Henry, T. J., Hambly, N. C., Brown, M. A., & Jao, W. 2005a, *AJ*, 129, 413, doi: [10.1086/426334](https://doi.org/10.1086/426334)
- Subasavage, J. P., Henry, T. J., Hambly, N. C., et al. 2005b, *AJ*, 130, 1658, doi: [10.1086/444540](https://doi.org/10.1086/444540)
- Teixeira, R., Ducourant, C., Chauvin, G., et al. 2009, *A&A*, 503, 281, doi: [10.1051/0004-6361/200912173](https://doi.org/10.1051/0004-6361/200912173)
- Thackeray, W. G. 1917, *MNRAS*, 77, 204
- Tinney, C. G., Reid, I. N., Gizis, J., & Mould, J. R. 1995, *AJ*, 110, 3014, doi: [10.1086/117743](https://doi.org/10.1086/117743)
- Torres, C. A. O., Quast, G. R., da Silva, L., et al. 2006, *A&A*, 460, 695, doi: [10.1051/0004-6361:20065602](https://doi.org/10.1051/0004-6361:20065602)
- Turnshek, D. E., Turnshek, D. A., Craine, E. R., & Boeshaar, P. C. 1985, *An atlas of digital spectra of cool stars (Types G, K, M, S and C).* (Western Research Company, 2030 E. Speedway Suite 213, Tucson, Arizona 85719, USA. 6+17 pp.+75 charts. Price US\$ 30.00 (1985). ISBN 0-934525-00-5.)
- Turon, C., Creze, M., Egret, D., et al. 1993, *Bulletin d'Information du Centre de Données Stellaires*, 43, 5

- van Leeuwen, F., ed. 2007, *Astrophysics and Space Science Library*, Vol. 350, *Hipparcos, the New Reduction of the Raw Data*, ed. F. van Leeuwen (Berlin: Springer)
- Voges, W., Aschenbach, B., Boller, T., et al. 1999, *A&A*, 349, 389
- . 2000, *IAU Circ.*, 7432, 1
- Walt, S. v. d., Colbert, S. C., & Varoquaux, G. 2011, *Computing in Science & Engineering*, 13, 22, doi: <http://dx.doi.org/10.1109/MCSE.2011.37>
- Webb, R. A., Zuckerman, B., Platais, I., et al. 1999, *ApJ*, 512, L63, doi: [10.1086/311856](https://doi.org/10.1086/311856)
- West, A. A., Hawley, S. L., Bochanski, J. J., et al. 2008, *AJ*, 135, 785, doi: [10.1088/0004-6256/135/3/785](https://doi.org/10.1088/0004-6256/135/3/785)
- Westerlund, B. E., Olander, N., & Hedin, B. 1981, *A&AS*, 43, 267
- White, R. J., & Basri, G. 2003, *ApJ*, 582, 1109, doi: [10.1086/344673](https://doi.org/10.1086/344673)
- Winters, J. G., Henry, T. J., Lurie, J. C., et al. 2015, *AJ*, 149, 5, doi: [10.1088/0004-6256/149/1/5](https://doi.org/10.1088/0004-6256/149/1/5)
- Winters, J. G., Sevrinsky, R. A., Jao, W.-C., et al. 2017, *AJ*, 153, 14, doi: [10.3847/1538-3881/153/1/14](https://doi.org/10.3847/1538-3881/153/1/14)
- Wroblewski, H., & Torres, C. 1989, *A&AS*, 78, 231
- Zacharias, N., Finch, C. T., Girard, T. M., et al. 2013, *AJ*, 145, 44, doi: [10.1088/0004-6256/145/2/44](https://doi.org/10.1088/0004-6256/145/2/44)
- Zuckerman, B., & Song, I. 2004, *ARA&A*, 42, 685
- Zuckerman, B., Song, I., & Webb, R. A. 2001, *ApJ*, 559, 388, doi: [10.1086/322305](https://doi.org/10.1086/322305)